Degradation Mechanisms of Pigmented Coatings

Ohio State University

prepared for

Air Force Materials Laboratory

OCTOBER 1972

AFML-TR-71-42
PART II

AD 753410

DEGRADATION MECHANISMS OF PIGMENTED COATINGS

William B. Campbell, Ph.D.
Joe K. Cochran, Jr., Ph.D.
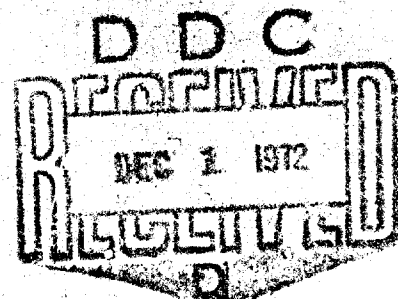
The Ohio State University
Research Foundation

TECHNICAL REPORT AFML-TR-71-42, PART II

October 1972

Approved for public release; distribution unlimited.

Air Force Materials Laboratory
Air Force Systems Command
Wright-Patterson Air Force Base, Ohio 45433

DOCUMENT CONTROL DATA - R & D

(Security classification of title, body of abstract and indexing annotation must be entered when the overall report is classified)

1 ORIGINATING ACTIVITY *(Corporate author)*	2a. REPORT SECURITY CLASSIFICATION
Ohio State University Research Foundation 1314 Kinnear Rd. Columbus, Ohio 43212	UNCLASSIFIED
	2b. GROUP N/A

3 REPORT TITLE

DEGRADATION MECHANISMS OF PIGMENTED COATINGS

4 DESCRIPTIVE NOTES *(Type of report and inclusive dates)*

Final   1 January 1971 - 30 August 1972

5. AUTHOR(S) *(First name, middle initial, last name)*

William B. Campbell
Joe K. Cochran

6. REPORT DATE	7a. TOTAL NO. OF PAGES	7b. NO. OF REFS
October, 1972	88	97

8a. CONTRACT OR GRANT NO	9a. ORIGINATOR'S REPORT NUMBER(S)
F33615-71-C-1257	
b. PROJECT NO. 7342	
c. Task No.	9b. OTHER REPORT NO(S) *(Any other numbers that may be assigned this report)*
d. 734202	AFML-TR-71-42, Pt II

10. DISTRIBUTION STATEMENT

Approved for public release; distribution unlimited.

11. SUPPLEMENTARY NOTES	12 SPONSORING MILITARY ACTIVITY
TECH, OTHER	Air Force Materials Laboratory (MBE) Air Force Systems Command (AFSC) Wright-Patterson AFB Ohio 45433

13 ABSTRACT

Oxygen transport in polymonomethylsiloxane was investigated and compared to polydimethylsiloxane properties. The effects of rutile pigmentation on the permeability, diffusion, and solubility of oxygen through polymonomethylsiloxane were investigated. Permeability and diffusion constants decreased with increasing pigment concentration and there was no evidence of oxygen sorption on the pigment.

Relative adhesion of polydimethylsiloxane and polymonomethylsiloxane on rutile was predicted from water contact angles. Polymonomethylsiloxane was proposed to have the greater adhesion but was small in either case.

The stability of dimethyl and monomethyl polysiloxanes pigmented with rutile and zinc oxide was evaluated in a simulated solar ultraviolet environment. Oxygen transport properties of the selected polymers were not observed to limit damage of eith pigment. Degradation of silicone/rutile paints was attributable to independent optical damage in the pigment and polymer. The silicate-coated rutile exhibited small reflectance changes as reported for other silicate coated pigments.

Ultraviolet degradation of zinc orthotitanate powders exhibited no dependence on either pigment particle size or quenching temperature. The initial solar absorptance increased with increased quenching temperature.

Ia

DD FORM 1473
1 NOV 65

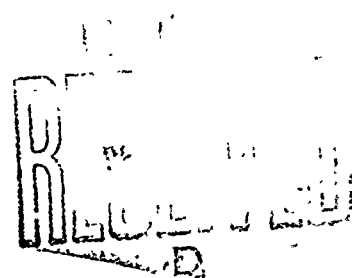| 14. KEY WORDS	LINK A		LINK B		LINK C	
	ROLE	WT	ROLE	WT	ROLE	WT
U.V. Space Degradation						
Thermal Control Coatings						
Zinc Oxide						
Polymonomethylsiloxane						
Polydimethylsiloxane						
Diffusion in Polymeric Coatings						
Silicone Rutile Paints						
Zinc Orthotitanate						
Rutile						
Solar Absorptance						

Ib

AFML-TR-71-42
PART II

DEGRADATION MECHANISMS OF PIGMENTED COATINGS

William B. Campbell, Ph.D.
Joe K. Cochran, Jr., Ph.D.

IC

FOREWORD

This report was prepared by Ohio State University Research Foundation under Air Force Contract F33615-71-C-1257. The contract was initiated under Project No. 7342, "Fundamental Research on Macromolecular Materials and Lubrication Phenomena," Task No. 734002, "Studies on the Structure-Property Relationship of Polymer Materials." The work was administered under the direction of the Elastomers and Coatings Branch, Nonmetallic Materials Division, Air Force Materials Laboratory, with Dr. William L. Lehn serving as Project Engineer. This report describes work conducted between 1 January 1971 and 30 August 1972. This report was released by the authors in September 1972 for publication as a Technical Report.

This technical report has been reviewed and is approved.

WARREN P. JOHNSON, Chief
Elastomers and Coatings Branch
Nonmetallic Materials Division
Air Force Materials Laboratory

ii

ABSTRACT

Oxygen transport in polymonomethylsiloxane was investigated and compared to polydimethylsiloxane properties. The effects of rutile pigmentation on the permeability, diffusion, and solubility of oxygen through polymonomethylsiloxane were investigated. Permeability and diffusion constants decreased with increasing pigment concentration and there was no evidence of oxygen sorption on the pigment.

Relative adhesion of polydimethylsiloxane and polymonomethylsiloxane on rutile was predicted from water contact angles. Polymonomethylsiloxane was proposed to have the greater adhesion but was small in either case.

The stability of dimethyl and monomethyl polysiloxanes pigmented with rutile and zinc oxide was evaluated in a simulated solar ultraviolet environment. Oxygen transport properties of the selected polymers were not observed to limit damage of either pigment. Degradation of silicone/rutile paints was attributable to independent optical damage in the pigment and polymer. The silicate-coated rutile exhibited small reflectance changes as reported for other silicate coated pigments.

Ultraviolet degradation of zinc orthotitanate powders exhibited no dependence on either pigment particle size or quenching temperature. The initial solar absorptance increased with increased quenching temperature.

TABLE OF CONTENTS

Preceding page blank

TABLE OF CONTENTS (Continued)

LIST OF ILLUSTRATIONS

LIST OF TABLES

DEGRADATION MECHANISMS OF PIGMENTED COATINGS

I. INTRODUCTION

Stringent temperature control for spacecraft is necessary to protect man and temperature-sensitive electronic equipment. The exchange of radiant energy between the vehicle and space, the principal means for temperature regulation, is controlled by the optical properties of the surface of the spacecraft. For space travel near the earth, coatings have been applied with a low solar absorptance (α_s) to infrared emittance (ϵ) ratio. Thermal control coatings are white and consist of oxide pigments of high index of refraction dispersed in a polymeric binder of low refractive index. Unfortunately, coatings of this type are damaged when exposed to high energy bombardment (solar ultraviolet radiation, protons, and electrons) in space. The damage produces an increase in the solar absorptance of the paint.

Much work has been directed toward identification of the degradation mechanisms. If the causes of degradation were understood, coatings which are stable or, at least, degrade in a predictable manner, might be developed. Degradation has been observed in the pigment and the polymeric binder; however, binders now exhibit minimal degradation and the major goal remains to develop a stable pigment.

Radiation produced defects which absorb photon energies in the solar spectrum are the cause of optical degradation in oxide pigments. The identification of the absorbing defects has received considerable attention. For the purpose of this investigation, the exact absorbing species is unimportant but in all cases the formation of absorbing species is accompanied by the photodesorption of oxygen. Thus, the oxygen transport properties of polymer encapsulants will influence pigment stability.

In some cases, polymeric binders have substantially influenced the degradation of thermal control coatings but the interaction of the pigment and the polymer has not been established. Suggestions of pigment surface passivation by the encapsulating medium has warranted consideration of the pigment-polymer interface stability. The surface condition of the pigment has been regarded as being a prime consideration in understanding degradation.

The purposes of this investigation are to determine pigment degradation dependence on (1) oxygen transport in typical polymeric binders, (2) pigment/polymer surface compatibility, (3) pigment surface area, and (4) heat treatment.

II. TECHNICAL DISCUSSION

1. Solar Reflectance and Absorptance

The effect of optical parameters on solar reflectance, R_s, and solar absorptance, α_s, may be defined by measurement principles. Solar reflectance is measured for calculation of solar absorptance and their sum is unity,

$$R_s + \alpha_s = 1 \tag{1}$$

Reflectance is measured as a function of wavelength and relative to a suitable white standard such as MgO, $MgCO_3$, or $BaSO_4$. The reflectance of the standard is assumed to be one, $R_{\infty Std} = 1$. The subscript denotes a sample sufficiently thick to prevent transmission; in practice, typical standards have a reflectance of 0.98 to 0.99.[1] The reflectance of typical thermal control pigments is shown in Fig. 1.

Solar reflectance over the solar spectrum[2] may be calculated from

$$R_s = \int I_{s\lambda} R_\lambda d\lambda \tag{2}$$

where $I_{s\lambda}$ is the solar radiation intensity at a specific wavelength and R_λ is the resulting reflectance.[3] At any wavelength, solar reflectance is proportional to solar radiation intensity. In practice, the solar spectrum is incremented into n equal energy bands, and solar reflectance is calculated from

$$R_s = \sum_{i=1}^{n} R_i/n \tag{3}$$

where R_i is the average reflectance.

2. Flight Evaluations of Coatings

Until 1965, the solar absorptance of oxide pigments, such as ZnO and TiO_2, was thought to increase only slightly by exposure to ultraviolet radiation. In the laboratory, the most stable thermal control coating was polydimethylsiloxane pigmented with zinc oxide which later proved extremely unstable. Before 1965, optical stability was determined by measuring the solar reflectance before and after ultraviolet irradiation in a vacuum but with post-irradiation reflectance measurements in air.

The first serious discrepancies were reported by Pearson[4] for data collected on Orbiting Solar Observatory II. Solar absorptances of

Preceding page blank   3
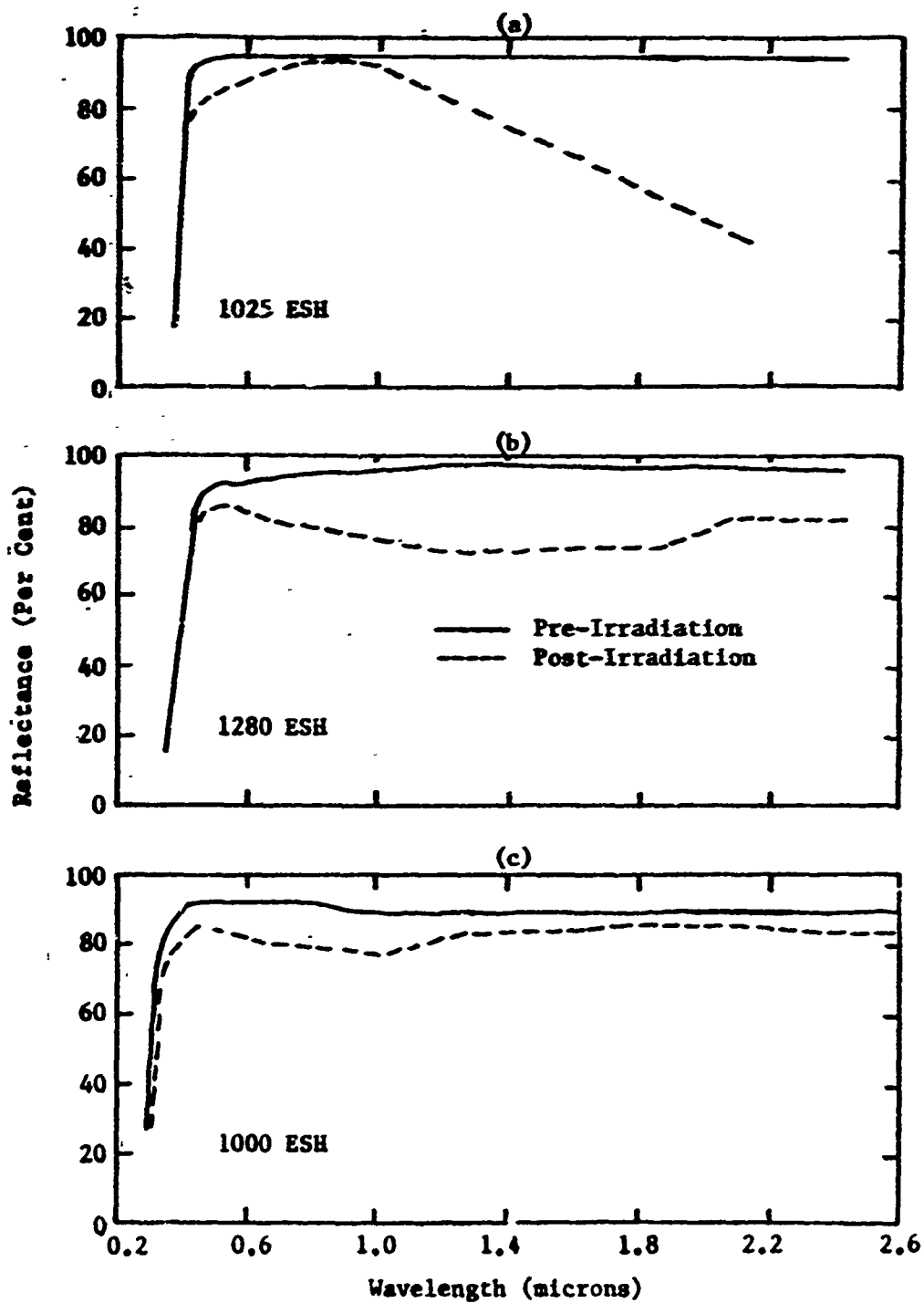
Figure 1. Typical Ultraviolet Degradation of (a) Zinc Oxide, (b) Rutile, and (c) Zinc Orthotitanate at Five Suns Intensity

titanium dioxide and zinc oxide in silicone binders increased at rates greater than laboratory predictions. Confirming data were obtained on the Mariner IV flight where zinc oxide in potassium silicate degraded at ten times the laboratory rates.[5] The flight-laboratory discrepancies were demonstrated by MacMillan et al. by decreased reflectance under vacuum and ultraviolet irradiation.[6] Subsequent measurements of reflectance under vacuum were referred to as in situ.

Zinc oxide and titanium dioxide, both in polydimethylsiloxane, exhibited increases of 0.10 and 0.15, respectively, in solar absorptance, $\Delta\alpha_s$, at 1330 equivalent sunlight hours, ESH. No further absorptance changes occurred on termination of ultraviolet irradiation, but within ten minutes of air admission, induced solar absorptance decreased to 0.01 for zinc oxide and to 0.03 for titanium dioxide. The solar absorptance recovery to near pre-irradiation values invalidated many previous radiation damage concepts. A description of in situ reflectance apparatus was reported by Zerlaut and Courtney.[7]

Since radiation-induced solar absorptance bleaches rapidly by exposure to air, a number of flight experiments were designed to test laboratory in situ measurements. Data from Pegasus I and OSO-II (both near-earth orbit spacecraft) agreed well with laboratory results for a zinc oxide and polydimethylsiloxane coating.[8] Flight-laboratory correlation was shown to be highly dependent on the laboratory ultraviolet radiation source. Samples from the near-earth orbit of OSO-III correlated well for zinc oxide degraded with a mercury arc lamp while xenon radiation produced much higher optical damage than found in flight.[9] This was surprising because xenon radiation matches the solar spectrum better than a mercury arc, and induced absorptance is highly dependent on the spectrum of the radiation source.[10]

For deep space flights (the Mariner and Lunar Orbital series), solar absorptance increases were much greater. Increased degradation was attributed to increased particulate radiation (solar electrons and protons) found in deep space. Particulate radiation is negligible for near-earth flights and prediction of thermal control responses from laboratory testing is reliable. Deep space simulation using combinations of electrons, protons, and solar ultraviolet radiation has been poor due to the inability to duplicate the solar radiation environment and the synergistic effects of combined irradiation.[11,12]

3. Degradation and Damage Mechanisms

The evolution of oxygen from oxide pigments by the combination with photo-induced defects is necessary for most proposed mechanisms of ultraviolet degradation. The strongest evidence for relating ultraviolet-induced reflectance decreases to oxygen desorption has been the recovery of reflectance to pre-irradiation values with oxygen admission.

a. Zinc Oxide

Optical damage in zinc oxide occurs in two distinct regions, the visible (0.4-0.8 microns) and the infrared (above 0.8 micron). Damage in the infrared region rapidly and completely bleaches upon exposure to air while damage in the visible shows very little recovery. The infrared damage spectra can be regenerated by vacuum and may be observed for several cycles of air and vacuum exposure. It is related to the loss and gain of physically adsorbed oxygen.[13]

Photodesorption of oxygen has been related to photoconductivity in zinc oxide. Increases in system pressure and conductivity occurred simultaneously with tungsten irradiation. Desorbed oxygen was presumed responsible for pressure increases.[14] Oxygen was shown to be photodesorbed from irradiated zinc oxide, but manometric measurements prevented gas species identification. The absorbed oxygen species were postulated to be O_2^-, O^-, and O^{2-} with the relative quantities dependent on temperature.[15] By electrical conductivity and pressure measurements, the predominant absorbed species at room temperature was deduced to be O^-.[16]

Zinc oxide has a negative surface charge produced by the chemisorption of molecular oxygen on the surface as depicted in equation (4),[17]

$$\tfrac{1}{2} O_2(g) + e^- \rightarrow O^- . \tag{4}$$

Oxygen adsorption concentrates excess electrons at the surface and produces an electron deficient region extending approximately 100 to 1000 Å from the surface.[18] Further evidence for surface degradation was the lack of detectable damage in single crystal zinc oxide.[19]

Radiation induced holes, attracted to the surface by the negative charge, combine with chemisorbed oxygen to form physically adsorbed oxygen. Samll attractive forces (0.05 eV) permit thermal oxygen desorption. Under vacuum, desorption is irreversible and excess zinc is deposited at the surface to reverse the charge. Holes must overcome a retarding potential before the defect concentration reaches equilibrium. Thus, induced absorptance reaches a constant value for a specific set of conditions. Degradation rate may seem to be initially limited by oxygen desorption and later by hole arrival at the surface.[19]

Blakemore assumed that interstitial zinc was responsible for increased solar absorptance.[20] Sklensky, et al. proposed induced infrared absorption by either free carrier electrons or oxygen vacancies (F-centers). Free carrier absorption was eliminated because free electrons were not detected by electron spin resonance and absorption did not increase as the third power of wavelength. Visible absorption was attributed to either lattice distortion stemming from excess zinc or hole traps. Lack of visible spectrum recovery was in agreement with diffusion of zinc to produce lattice strain.[21]

Morrison and Freund proposed that excess zinc precipitated at dislocations. The resulting lattice strain would cause the absorption edge to develop a tail extending into the visible and infrared or absorption by a complex zinc-dislocation color center would occur. They supported the dislocation theory by inducing surface dislocations in single crystal zinc oxide to produce a band edge shift indistinguishable from the photodegradation shift.[22]

b. Rutile

Rutile degradation is similar to zinc oxide with absorption from the absorption edge into the infrared and a maximum from approximately 0.8 to 2.0 micron. Recovery of rutile is incomplete with greater permanent damage remaining in the visible than in the infrared.[23] No measurable absorption increase for single crystal rutile is in accord with a calculated electron depletion depth of 2000 Å.[24]

Oxygen adsorption-desorption degradation control has been suggested for rutile. Correlation has been established between increased solar absorptance and increases in carbon dioxide pressure evolved from rutile containing in excess of 100 ppm carbon.[25] An increase in oxygen pressure was observed during the peak degradation rate of rutile, but the quantity of oxygen was too small to clearly distinguish between adsorbed and desorbed oxygen.[25]

A large number of defects have been suggested; among them are F-centers, interstitial titanium, and Ti^{+3}.[27] Greenberg, et al. suggested that the broadness of the absorption band resulted from several combined defects such as $(e/O_V^{-2}/Ti^{+3})^0$, (O_V^{-2}/Ti^{+3}), or $(Ti^{+3}/O_V^{-2}/Ti^{+3})^0$.[28] Coufova and Arend studied the optical absorption spectrum by annealing rutile in hydrogen and attributed absorption peaks at 0.5 and 0.66 micron to electrons at oxygen vacancies.[29] Von Hipple, et al. observed absorption at 1.5 microns in oxygen-deficient rutile and concluded it was caused by lattice collapse from oxygen loss, allowing Ti^{+4} to trap electrons and form Ti^{+3} near oxygen vacancies.[30] Yahia measured electrical conductivity of rutile as a function of oxygen pressure at 1000°K.[31] For pure rutile, an oxygen vacancy mechanism was predominant above 10 mmHg and titanium interstitials dominated below 10 mmHg. For Al-doped rutile, both mechanisms were present but could not be separated.

c. Zinc Orthotitanate

Zinc orthotitanate exhibits ultraviolet-induced absorption similar to rutile except the peak degradation occurs at 0.85 micron. Through electron paramagnetic resonance studies, Ashford and Zerlaut concluded that Ti^{+1} was created by photodesorption of oxygen and is responsible for induced absorption in zinc orthotitanate.[32]

d. Polymethylsiloxanes

Silicones have received widespread use as a binder in thermal control coatings. Polydimethylsiloxane, $[(CH_3)_2SiO]_n$, and polymonomethylsiloxane, $[CH_3SiO_{1.5}]_n$, have absorption edges near 0.2 micron and are transparent in the remainder of the ultraviolet and the visible spectrum. Both silicones exhibit absorption increases in the ultraviolet and shortwave portion of the visible spectrum after exposure to solar environment. Polymonomethylsiloxane is thermally cured and is more stable. The greater degradation of the dimethylsiloxane results from damage to the catalyst used in curing.[34] Recent evidence indicates that the instability of the dimethyl form is not caused by curing agents but by silicone decomposition or trace contamination.[35]

In paints, silicone degradation is minor compared to pigment degradation. Pigmentation with ultraviolet absorbent materials provides additional protection for the binder by screening. Thus, the major effort in improving the solar stability of thermal control coatings has been directed toward pigments.

Comparison of binderless pigments with paints indicate improved degradation resistance from the silicone binders. A rutile polydimethylsiloxane paint showed (1) infrared absorptance increases to be lower and slower for the paint than the pigment, (2) paint degradation to increase with temperature, and (3) increasing the ultraviolet intensity increased pigment degradation while paint degradation remained insensitive.[36] These results suggested that oxygen transport through the binder may limit degradation. In a similar investigation of rutile-silicone paints and binderless pigments, recovery rates suggested diffusion-limited kinetics for the paints. Also the binder appeared to have a passivating effect on the pigment.[37]

4. Pigment Surface Stabilization

Single crystals exhibit no increase in solar absorptance, while corresponding pigments with surface areas four orders of magnitude greater degrade severely. Similarly, larger particles exhibit less degradation for the same volume concentration than smaller ones.[38] Increased degradation rates may be attributed to increased lattice strains and increased surface defect states produced in grinding.[39] The radiation induced defects may be confined to the electron depleted region near the surface of each particle. Pigments with a radius smaller than the depletion depth degrade in bulk, while the solar absorptance of larger particles remain unchanged at a core.

The importance of improving pigment surface stability led to various passivation processes. The most widely referenced passivation was zinc oxide with potassium silicate in aqueous solution.[40] Silicate-coated zinc oxide became one of the most ultraviolet stable thermal control coatings produced to date.[41] Zerlaut, et al. reported that

the silicate replaced surface oxygen and prevented oxygen photodesorption.[42] This mechanism suggested chemical passivation but Szlensky, et al. concluded that silicate coating may physically inhibit oxygen transport.[43] A similar silicate coating is commonly used on terrestrial rutile pigment to improve the resistance to ultraviolet discoloration and fading.[44] The coating is precipitated from aqueous sodium silicate and calcined at 400°-600°C.[45] Approximately 1% of zinc oxide is also precipitated from a zinc sulfate solution during the coating process.[46]

Titania-opacified porcelain enamels have extreme stability in an ultraviolet environment, and even high degradable antimony oxide exhibits surprising stability in an enamel. The stabilization of an enamel may involve either chemical passivation and/or physical inhibition of oxygen photodesorption. Low oxygen diffusion in glasses promote physical passivation even in the absence of chemical stabilization.

5. Mass Transport in Polymers

For steady state flow of a gas through a membrane of thickness, ℓ, the permeability coefficient, P, is defined as

$$J = P\,(p_1 - p_2)/\ell \tag{5}$$

where J is the flux per unit membrane area perpendicular to the direction of flow, p_1 is the gas pressure on the high pressure side of the membrane and p_2 is the pressure on the low pressure side.[48] For experimental simplicity $p_2 \simeq 0$ and $p_2 \ll p_1$, so that $p_1 - p_2 \simeq p_1$. If Henry's law is valid over the pressure region, the solubility coefficient, S, is

$$C = Sp \tag{6}$$

where C is concentration.[49] For conditions of equilibrium at the gas polymer interface, the steady state diffusion coefficient, D, is given by Fick's first law.

$$J = DC/\ell \tag{7}$$

and by combining equations (5) - (7), the relation between P, D, and S is

$$P = DS. \tag{8}$$

For diffusion in a pure polymer the diffusion coefficient is equal to the interdiffusion coefficient, D_{12}, for the gas-polymer mixture. If Henry's law is valid for the gas-polymer solution, there is no chemical activity correction, and if the gas solubility is dilute with respect to the diffusion gases, then

$$D = D_{12} \simeq D_1 \simeq D_1^* \tag{9}$$

where D_1 and D_1^* are the intrinsic and self-diffusion coefficients of the gas in the gas-polymer mixture.[50] When the high pressure is maintained constant, the gas concentration in the membrane is initially zero and the gas permeates into an evacuated constant volume, the low pressure will increase with a continually increasing rate until a steady state pressure rate is reached, Fig. 2. Extrapolation of the steady state pressure-time curve to the time axis establishes the lag time, L, which is used to calculate the diffusion coefficient from,[51]

$$D = \ell^2/6L. \tag{10}$$

The steady state pressure rate, dP/dt, is used in determining the permeability constant, P. Determinations of the diffusion coefficient from time lag and the permeability constant from steady state measurements have been used extensively to determine gas permeability, diffusion, and solubility in polymers.

Permeability, diffusion and solubility are exponentially related to temperature according to the Arrhenius relationships,

$$P = P_o \, \exp\text{-}(E_p/RT), \tag{11}$$

$$D = D_c \, \exp\text{-}(E_D/RT), \tag{12}$$

and
$$S = S_o \, \exp\text{-}(\Delta H_s/RT), \tag{13}$$

where P_o, D_o, and S_o are pre-exponential factors, E_p and E_D are activation energies for permeability and diffusion, respectively, and ΔH_s is the heat of solution.[52] Substitution of equations (11) to (13) into equation (8) gives the relation between E_p, E_D, and ΔH_s,

$$E_p = E_D + \Delta H_s. \tag{14}$$

Equations (11) to (13) have been shown to be valid for simple gases in many polymers over limited temperature ranges.[53,54]

Activation energies for diffusion are dependent on the degree of crosslinking in polymers. As crosslinking increases in natural rubber by additions of sulfur, diffusion activation energies increase. The changes may be attributed to a reduction in the mobility of the polymer chains as crosslinking increased.[55]

Heats of solution for gases in polymers include the heat of mixing and heat of condensation. Both are small with the heat of mixing usually positive and the heat of condensation always negative. Thus, heats of solution may be positive or negative and are usually small.[56]
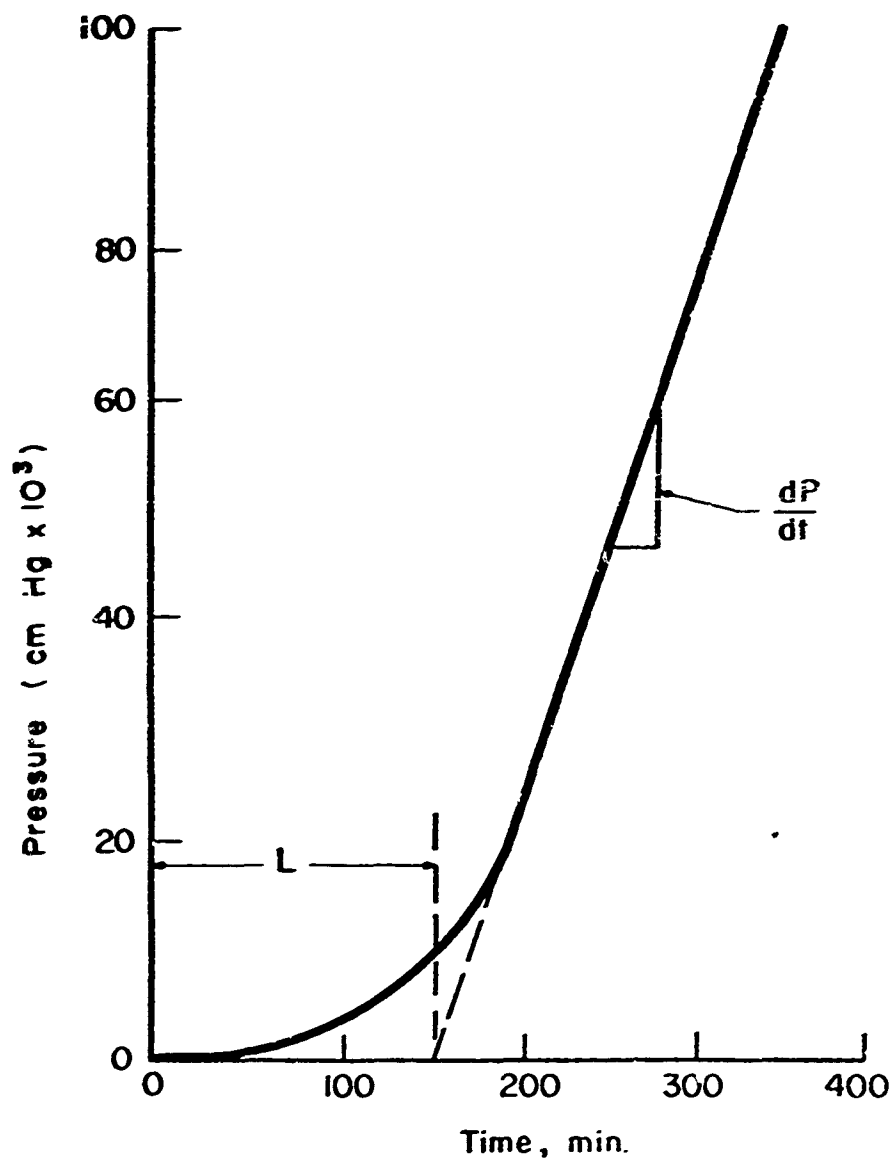
Figure 2. Typical Pressure-Time Curve for Measurement of
Gas Permeability and Diffusion

11

a. Polydimethylsiloxane

Polydimethylsiloxane (PDMS) consists of linear molecules based on the $(CH_3)_2SiO$ unit shown below.[57]

$$
\begin{array}{ccccccc}
& CH_3 & & CH_3 & & CH_3 & \\
& | & & | & & | & \\
-Si & - & O-Si & - & O-Si & - & O- \\
& | & & | & & | & \\
& CH_3 & & CH_3 & & CH_3 &
\end{array}
$$
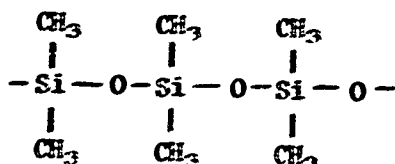
This elastomer remains amorphous to approximately -50°C where crystallization begins and continues to below -60°C.[58] A low energy barrier allows free rotation of CH_3 groups about siloxane bonds[59] and results in high gas mobilities in the elastomer.[60,61] Solubilities of gases in PDMS are similar to those in natural rubber although diffusion and permeability coefficients are at least an order of magnitude greater.[62]

Barrer and Chio measured oxygen permeability, diffusion, and solubility constants in polydimethylsiloxane filled with silica over the temperature range -40 to 0°C, Table I. The low activation energies for diffusion are associated with free rotation of methyl groups.

Table I - Oxygen Transport Constants for
Polydimethylsiloxane/Silica[63]

	T (°C)	Volume Per Cent Silica 5.54	18.2
$P \times 10^8$ (cc(STP)/sec/ cm^2/cm/cm Hg)	0	4.89	3.85
$D \times 10^6$ (cm^2/sec)	0	12.0	10.6
S (cc(STP)/cc/atm)	0	0.311	0.277
E_p (cal/mole)	-40 to 0	2070[a]	1870[a]
E_D (cal/mole)	-40 to 0	2160	3060
ΔH_S (cal/mole)	-40 to 0	-90[a]	-1190[a]

[a] Calculated

Comparison of E_D and D_o to those for self-diffusion in liquids indicated that polydimethylsiloxane is more comparable to liquids than other elastomers. Higher activation energy for diffusion at the higher filler concentration was attributed to the filler particles acting as crosslinking agents and producing a tighter chain network.[63]

b. Effect of Pigmentation

Solubility--Where the binder and the pigment in thermal control coatings can be considered separate, noninteracting phases, the gas solubility coefficient of the paint in the absence of pores can be expressed as

$$S = V_B S_B + V_p S_p \qquad (15)$$

where V_B and V_p are the volume fractions of binder and pigment, respectively, S_B is the solubility coefficient of binder, and S_p is the surface adsorption coefficient of the pigment. Should porosity be present in the pigmented polymer, the quantity of gas occupying the pore would be added to equation (15), giving,

$$S = V_B S_B + V_p S_p + V_v S_v \qquad (16)$$

where V_v is the volume fraction of pores or voids and S_v is the solubility coefficient. If there are no voids and the polymer wets the pigment to the exclusion of gas adsorption, the solubility of the composite will be represented by equation (15) with S_p equal to zero.[64] If the pigment is not completely wet by the polymer, an extensive interface is created for gas adsorption. For natural rubber filled with carbon black, the hydrogen, nitrogen, and oxygen solubilities in the composite were greater than predicted for rubber alone.[65]

Barrer, et al. investigated solubility of propane at 40°C in natural rubber filled with 0 to 40 volume per cent zinc oxide. At low filler concentrations, propane solution occurred in the rubber only; as pigment concentration increased, filler adsorption and solubility was well represented by equation (15). The porosity at higher pigment concentrations was associated with aggregates which prevented wetting by the polymer.[66]

Solubility of C_4 and C_5 paraffins in silicone rubber filled with 0 to 19 volume per cent silica was predicted by equation (15) with silica adsorption equal to zero. An investigation of temperature effects showed no variation in heats of solution with filler concentration.[67]

Diffusion--Diffusion in a heterogeneous medium is a complex situation for which diffusion equations have not been derived. Instead, existing equations have been modified to take into account, among other things, increased path length due to the presence of the filler. Barrer, et al. reported for transient state flow,

13

$$\frac{\partial C}{\partial t} = V_B K D_B \frac{\partial^2 C_B}{\partial x^2} \qquad (17)$$

which can be compared to Fick's Second Law where D is not a function of position,

$$\frac{\partial C}{\partial t} = D \frac{\partial^2 C}{\partial x^2} \qquad (18)$$

where C and C_B are concentration in the pigmented polymer and polymer, respectively; t is time; K is a structure factor; D and D_B are the diffusion coefficients in the pigmented polymer and polymer, respectively. The concentration of gas in the pigmented polymer excluding the pore phase is

$$C = V_B C_B + V_p C_p \qquad (19)$$

and if Henry's law holds for the pigment and the polymer,

$$C_p/C_B = S_p/S_B. \qquad (20)$$

Rearrangement of equation (19) and substitution of equation (20) gives,

$$C_B = \frac{C}{V_B + V_p(S_p/S_B)} . \qquad (21)$$

Therefore,

$$\frac{\partial^2 C_B}{\partial x^2} = \frac{1}{V_B + V_p(S_p/S_B)} \frac{\partial^2 C}{\partial x^2} \qquad (22)$$

and

$$D = K D_B \frac{V_B}{V_B + V_p(S_p/S_B)} \qquad (23)$$

If no adsorption occurs on the pigment,

$$D = K D_B \qquad (24)$$

Equations (17) through (24) are based on the assumptions that diffusion proceeds only in the polymer phase and diffusion in the polymer is unchanged by the filler.[68]

Rayleigh[69] in 1892, derived a structure factor predicting the influence of a cubic lattice of spheres on the properties of a medium. His factor has been successful[70,71] in explaining diffusion in heterogeneous media and can be expressed as

$$K = \frac{1}{V_B} \left(1 - \frac{3V_p}{2 + V_p - 0.392 V_p^{10/3}} \right) . \qquad (25)$$

14

Equation (25) makes no assumption on the size of particles present but only upon the volume fraction.

Permeability--Changes in permeability constants caused by pigmentation have been expressed using the structure factor of equation (25).[72] Since $D = P/S$, substitution into equation (23) gives,

$$\frac{P}{S} = K \frac{P_B}{S_B} \frac{V_B}{V_B + V_p(S_p/S_B)} \tag{26}$$

and on rearrangement,

$$P = K V_B P_B \frac{S}{V_B S_B + V_p S_p} \tag{27}$$

Substitution of equation (15) into (27) gives,

$$P = K V_B P_B , \tag{28}$$

where P_B is the permeability constant for the polymer. Equation (28) is valid whether or not adsorption occurs on the pigment.

6. Surface Energies, Contact Angle, and Adhesion

Equilibrium between the three surface energies in a system composed of a drop on a plane-solid surface is given by Young's equation.

$$\gamma_{SV} = \gamma_{SL} + \gamma_{LV} \cos \theta \tag{29}$$

where γ_{SV}, γ_{SL}, and γ_{LV} are the surface free energies of the solid-vapor, solid-liquid, and liquid-vapor interfaces, respectively, and θ is the solid-liquid-vapor contact angle measured through the liquid phase, Fig. 3. Of the four parameters only γ_{LV} and θ are experimentally determinable. The surface free energy of the liquid-vapor interface is the surface tension of the liquid in equilibrium with its vapor and the contact angle can be measured by a variety of techniques.[73]

The wettability of a solid by a liquid is indicated by contact angle. If a solid is not completely wet, the liquid contact angle is greater than zero and if complete wetting or spreading occurs, the contact angle is equal to zero. Conditions for spreading are given by

$$S = \gamma_{SV} - (\gamma_{SL} + \gamma_{SV}) \tag{30}$$

15
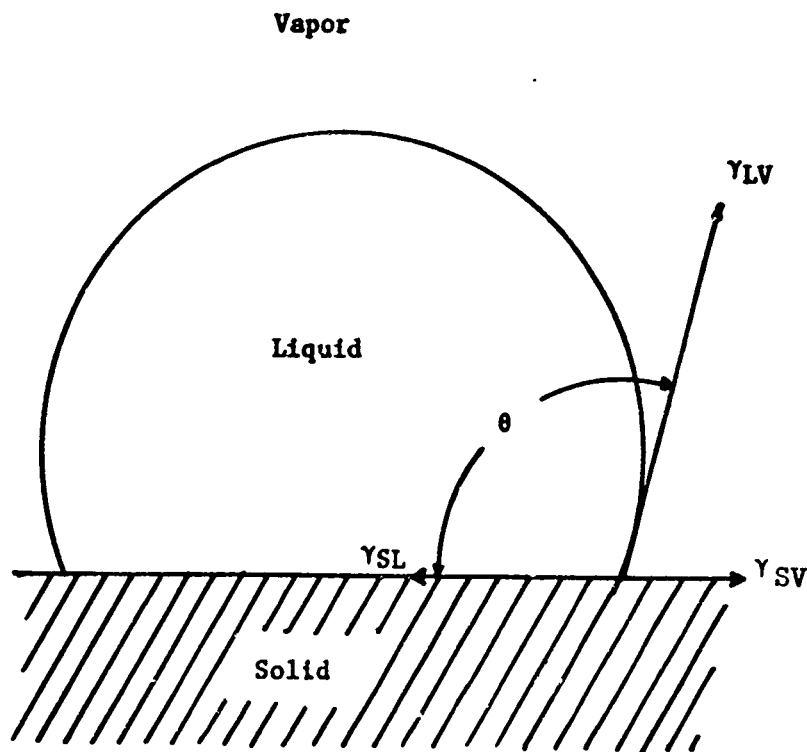
Vapor

Figure 3. Surface Energy/Contact Angle

where S is the spreading coefficient. For spreading to occur, S must be greater than zero. This simply means that the combined free energies of the solid-liquid and liquid-vapor interfaces must be less than the solid-vapor free energy. Under this condition the systems total free energy is reduced by eliminating as much of the solid-vapor interface as possible.[74]

The reversible work of separating a liquid from a solid is equal to the free energy change of the system,

$$W_A = \gamma_{SV} + \gamma_{LV} - \gamma_{SL} \tag{31}$$

where W_A is the work of adhesion. On substitution for γ_{SV} from Young's equation, the work of adhesion is

$$W_A = \gamma_{LV} (1 + \cos\theta). \tag{32}$$

Zisman presents a compilation of work of adhesion values and shows that the work of adhesion is a parabolic function of surface tension.[75]

Contact angles of liquids advancing over previously nonwetted surfaces may be very different from the receding angle. This has been attributed to the surface roughness of the solid. If gas is not trapped at the solid-liquid interface, contact angles less than 90° decrease with increasing surface roughness and angles greater than 90° increase.[76]

Strain in glass has been observed to have a sizeable effect on water contact angles. The contact angle of water on a clean glass is normally zero, but Bartell, et al. found water contact angles as high as 80° on glass that had been rapidly cooled. Examination of the glass with polarized light revealed intense strain. After strain removal by annealing, the contact angle returned to zero. Induced mechanical compression also caused an increase in contact angle.[77] The effect of gravity on contact angle is considered negligible and is generally ignored; however, differences in contact angles as much as 12° have been caused by gravity for a lucite-water-air system.[78]

Surfaces containing exposed methyl groups are hydrophobic and exhibit large contact angles with water. Highly condensed packing of methyl groups in crystallized paraffins have water contact angles as large as 111°, while the less densely packed methyl groups of amorphous paraffins have contact angles of 101°. An angle of 101° was found for polydimethylsiloxane which indicated that the methyl groups at the surface efficiently shielded the subsurface Si-O linkages.[79]

From studies of adhesives, it is generally found that polar surfaces will bond to polar surfaces and nonpolar to nonpolar. Glass with a negative surface charge has a polar surface and, consequently, it is wet by water. When bonding glass to glass, polymeric materials with polar functional groups such as -OH, -COOH, -C = O, and -COOCH$_3$ produce good adherence. For bonding polar surfaces to nonpolar surfaces, an intermediate coupling agent containing both polar and nonpolar functional groups is used. The polar groups of the coupling agent are oriented to the polar surface and nonpolar to the nonpolar.[80]

Moser has shown that adhesion between two materials can be predicted by determining the polarity of the surfaces using a water contact angle as an indicator. Surfaces wet by water were considered polar. As contact angles increased, the surfaces were considered more nonpolar and polarity ranges were arbitrarily defined as: 0 to 20°, polar; 21 to 45°, slightly nonpolar; 46 to 65°, moderately nonpolar; and 66 to 99° nonpolar. In general, similar polarity was necessary for good bonding. Where good bonding was obtained between surfaces of opposite polarity, a reorientation of the functional groups was evidenced by changes in water contact angles.[81-83]

III. EXPERIMENTAL PROCEDURE

1. Materials

a. Rutile Pigment

The pigment for contact angle studies and solar stability measurements was Ti-Pure R-992 Rutile, Lot 9980, from E. I. duPont deNemours and Company. This pigment was made by the chloride process and encapsulated with a silicate-zinc oxide coating from a sodium silicate-zinc sulfate aqueous solution before thermal treatment at 400-600°C. Typical chemical analysis of the final product is given in Table II.[84] The Al_2O_3 originated by oxidation of $TiCl_4$ and $AlCl_3$, was present in the pigment, not in the pigment coating.

Table II. Rutile Pigment Composition

Oxide	Weight Per Cent
TiO_2	89.5
Al_2O_3	1.01
SiO_2	5.8
ZnO	1.2

b. Zinc Oxide Pigment

New Jersey SP-500 zinc oxide was chosen for degradation rate studies.

c. Polydimethylsiloxane (PDMS)

The polydimethylsiloxane was RTV-602 from General Electric Company and was received with a typical viscosity of ten poises. After crosslinking with 1,1,3,3,tetramethylquanidene, a transparent elastomer was formed.

d. Polymonomethylsiloxane (PMMS)

An organopolysiloxane resin, OI-650 from Owens-Illinois, Inc., was dissolved in ethanol for paint preparation. Crosslinking by thermal treatment produced a brittle transparent solid. Ethanol and water were volatilized during curing, leaving polymonomethylsiloxane.[85]

Preceding page blank

2. Oxygen Transport

a. Measurement

Permeability constants were determined by the steady state method and diffusion coefficients by time lag. Solubility constants were calculated, $(S = P/D)$, where S, P, and D are solubility, permeability and diffusion constants, respectively. Apparatus and procedure have been described earlier.[96]

b. Sample Preparation

Polymonomethylsiloxane (PMMS) was dissolved in absolute ethanol at 40 per cent solids content. Citric acid was added at a concentration of one weight per cent of PMMS to reduce brittleness in the cured polymer.[97] PMMS/rutile compositions, Table III, were formulated using a polymer density of 1.298 and a pigment density of 4.066. Ethanol required to dissolve PMMS and thin the paints was added and paint volumes of 150 cc were dispersed by milling for 24 hours.

Samples were cast in 100-mm diameter glass rings on flat and level 0.013-cm Teflon sheets and covered with filter paper. Self-supporting membranes with glass rings attached were removed from the Teflon and cured vertically at 100°C for 48 hours. The glass rings supported the membranes during curing. Membrane thicknesses of approximately 0.02 cm had variations of six to seven per cent.

Table III. Compositions of Polymonomethylsiloxane
Pigmented with Rutile

| Composition | Weight Per Cent | | Volume Per Cent[a] | | |
	Rutile	PMMS	Rutile	PMMS	Ethanol[b]
11	85.3	14.7	94.8	5.2	200
12	73.3	26.7	89.6	10.4	200
13	55.0	45.0	79.3	20.7	200
14	41.6	58.4	69.0	31.0	200

[a] Volume per cents were calculated from measured densities of 1.298 and 4.066 for polymonomethylsiloxane and rutile, respectively.

[b] Ethanol volume percentages are based on rutile plus PMMS volumes of 100 per cent.

20

3. Contact Angle

a. Measurement

The wetting characteristics were determined by contact angle measurements of water drops. A cell with glass windows mounted to a horizontally positioned metallurgical microscope permitted vertical and horizontal positioning. Drops were illuminated with collimated light and recorded with a 35 mm camera.

Gravity effects were eliminated by measuring contact angles of a drop on the substrate (normal) and suspended from the substrate (inverted), Fig. 4. The substrate was mounted off-center and rotated on sealed ball bearings. The substrate position was fixed by a weight that could be adjusted to produce an exact 180° rotation.

The stage was parallel with the rotation axis. A bubble level mounted to the stage permitted leveling in the inverted position. Parallel surfaced substrates were positioned with spring loaded clips and could be rapidly rotated from the normal to the inverted position while maintaining a level sample surface.

A glass pipette containing distilled demineralized water was inserted through a compression O-ring seal in the top of the cell and lowered near the substrate surface. A container of water was placed in the cell and 30 minutes was allowed for atmosphere saturation. A drop was placed on the substrate and the pipette was retracted to prevent interference with sample inversion. Drops were allowed five minutes to equilibrate, photographed, then inverted rephotographed after five minutes, returned to normal, and photographed again after five minutes. Three drops on each of two samples of each material were measured. Drop reflection on the substrate surfaces gave a sharp delineation of the liquid-solid interface except for contact angles near 90°. Contact angles were measured with a goniometer on the enlarged projection of photograph negatives.

b. Sample Preparation

Water contact angles were measured on polycrystalline rutile, free-formed surfaces of PDMS and PMMS, rutile surfaces that were separated from cast PDMS and PMMS, and PDMS and PMMS surfaces separated from rutile. Free-formed surfaces were the air exposed surfaces of polymers cast on the low energy surface of Teflon and cured, as described for oxygen transport samples.

Silicate-coated, chloride-processed rutile pressed at 5000 psi as 2.8-cm discs was fired at 1115°C for 168 hours. Density of 95 + 0.1 per cent theoretical was obtained for six samples. Disc surfaces were diamond ground parallel to a thickness of 0.4 cm and one surface was polished to a 1µm diamond finish. Samples were cleaned by
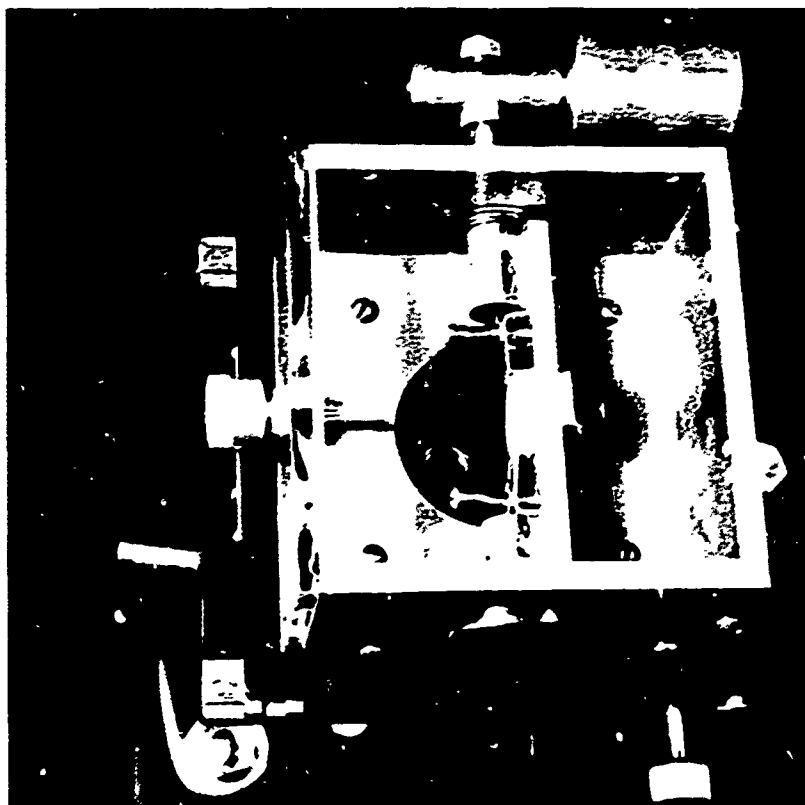
(a)   (b)
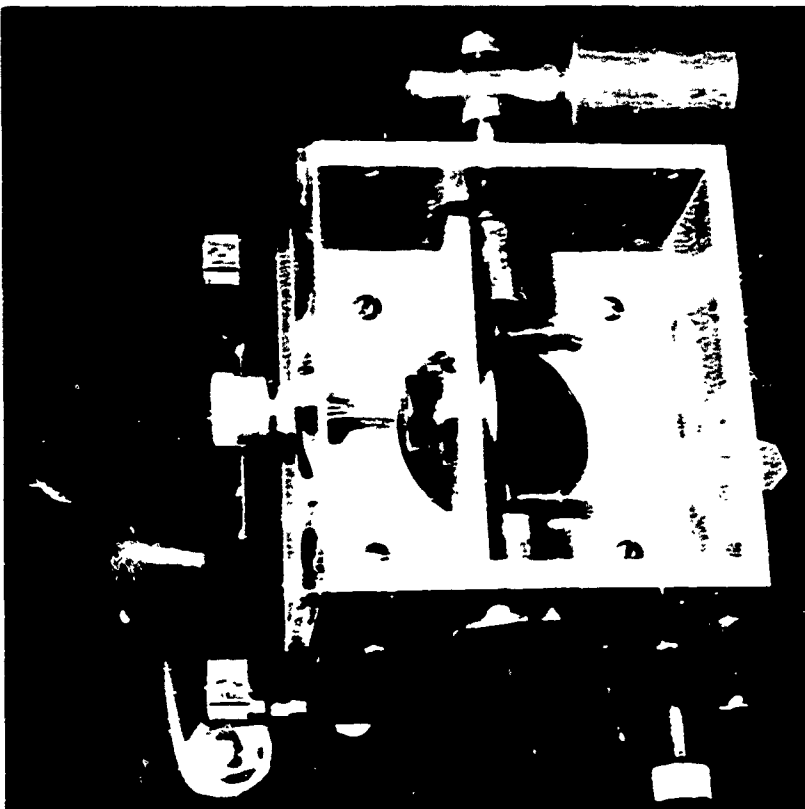
Figure 4. Contact Angle Measurement Apparatus; (a), Normal and (b) Inverted

boiling in 2:1 nitric-sulfuric acid, rinsing with large quantities of distilled water and drying at 120°C for five minutes. The complete spreading of water on a glass surface cleaned by this procedure was achieved.

PDMS and PMMS solutions prepared for mass transport were cast on cleaned rutile substrates and cured. Absence of adhesion allowed easy separation for measurement of the rutile/silicone interfaces. All samples involving silicones were evacuated at 10^{-7} torr for 24 hours to promote solvent removal.

4. In Situ Reflectance

a. Measurements

The effect of vacuum ultraviolet irradiation on the solar reflectance of polymethylsiloxane/zinc oxide paints was measured at the Elastomers and Coatings Branch, Wright-Patterson Air Force Base. Samples were irradiated with a 2.5 kW xenon source (Spectrolab Model X-25) at an ultraviolet intensity of two-thirds of one sun in a vacuum of 5×10^{-6} torr. Original ultraviolet intensity was estimated to be $3.0 + 0 - 0.3$ suns but on actual measurement was found to have the lower value because of severe degradation of the optical surfaces in the source unit. Reflectance was measured in situ with a Beckman DK-2A reflectometer using a four-inch integrating sphere in the vacuum chamber. Reflectance from 0.35 to 2.5 microns was measured in air before pumpdown. The samples were held in vacuum for one week and pre-irradiation vacuum reflectance was measured. In situ reflectance was measured periodically during irradiation and a recovery scan was made after two days in air. Solar reflectance, solar absorptance, and induced solar absorptance were calculated. Sample temperature varied from 60 to 80°C during irradiation.

b. Rutile Pigment and Paints Preparation

A rutile standard was prepared by spraying a water slurry of chloride-processed, silicate-coated rutile onto a heated aluminum substrate of 2.4 cm diameter and 0.88 cm thickness. Multiple layers produced a coating 0.0075 cm (3 mils) thick. Aluminum substrates were cleaned by abrading with 240-grit silicon carbide, rinsing in toluene and acetone, and drying. Rutile/silicone paint compositions 1-4, Table IV, and compositions 11-14, Table III, were cast to 0.003 cm (12 mils) and cured on the aluminum substrates. Paint preparation and and curing were the same as described for oxygen transport samples.[a,b] Citric acid was omitted from the PMMS paints.

Table IV. Compositions of Polydimethylsiloxane
Pigmented with Rutile

| Composition | Weight Per Cent | | Volume Per Cent[a] | | |
	Rutile	PDMS	Rutile	PDMS	Toluene[b]
1	18.72	81.28	5.36	94.64	34
2	31.97	58.03	10.36	89.64	34
3	52.22	47.78	21.17	78.83	50
4	64.61	35.59	30.78	69.22	66

[a]Volume per cents were calculated from measured densities of 0.999 and
4.066 for polydimethylsiloxane and rutile, respectively.

[b]Toluene volume percentages are based rutile plus PDMS volumes of 100
per cent.

c. Zinc Oxide Pigment and Paints Preparation

New Jersey SP-500 zinc oxide was chosen for degradation rate
studies. A zinc oxide standard was prepared by spraying a water slurry
on a precleaned aluminum substrate. Polydimethylsiloxane and polymono-
methylsiloxane were pigmented with 20 volume per cent zinc oxide and
cast on aluminum substrates. Paint preparation and curing were the same
as described for oxygen transport samples.

5. Zinc Orthotitanate Pigment

a. Pigment Formulation

Zinc orthotitanate pigments were prepared by ball milling and
heat treatment to obtain powders with a variety of particle sizes and
thermal histories. A flow chart of the pigment processing is presented
in Fig. 5.

In a five-gallon polyethylene jar, 3600 gm of a 2:1 molar
ratio of reagent grade ZnO and "iO$_2$ (anatase) were ball-milled with
9000 cc of demineralized, double-distilled water for 46 hours. The
slurry was dried, crushed to 60 mesh, and reacted for 24 hours at 925°C
in an alumina crucible. The resulting material, Sample A-1, contained
zinc orthotitanate and zinc oxide, as identified by x-ray diffracto-
meter, and had a particle size of 0.91 micron.

The reacted Zn$_2$TiO$_4$ was slurried with 4500 cc of 10% acetic
acid for 24 hours using a polyethylene stirrer. After settling, 4000 cc
of the sample was decanted, and the insoluble material was mixed with

24

2 ZnO + TiO₂ (3600 gm-ball milled 46 hr)
Dried and crushed to 60 mesh; reacted for
24 hr at 925°C; leached in 10% acetic acid;
divided into four 650-gm samples

Ball Milled 36 hr
d = 0.44 μm

Heat Treatment

850°C Anneal
850°C Quench
950°C Quench
1050°C Quench
1150°C Quench

Ball Milled 8 hr
d = 0.58 μm

Heat Treatment

850°C Anneal
850°C Quench
950°C Quench
1050°C Quench
1150°C Quench

Ball Milled 2 hr
d = 0.61 μm

Heat Treatment

850°C Anneal
850°C Quench
950°C Quench
1050°C Quench
1150°C Quench

No Milling
d = 0.80 μm

Heat Treatment

850°C Anneal
850°C Quench
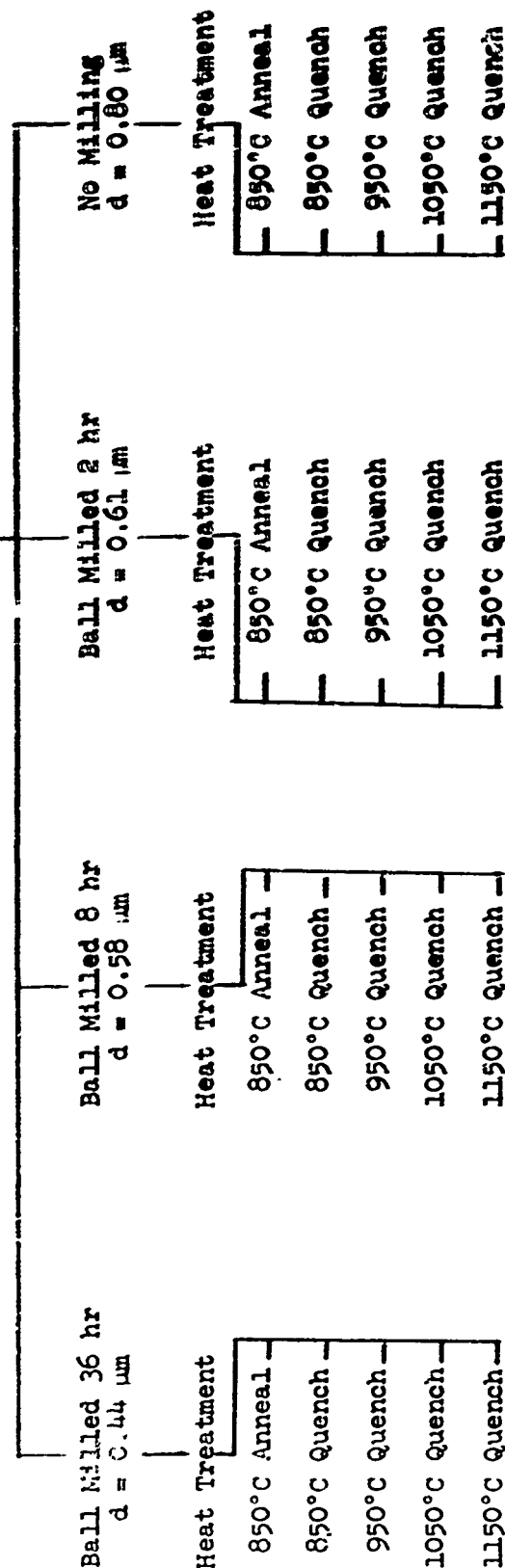950°C Quench
1050°C Quench
1150°C Quench

Figure 5. Flow Chart for Preparation of Zn₂TiO₄ Pigments

4000 cc of distilled water. The decanting process was repeated eight times and the final batch, Sample A-2, was dried at 120°C. Weight loss on leaching was 147 gm (4.0%) and the only x-ray diffractometer detectable peak other than Zn_2TiO_4 had an intensity less than 1%. The particle size of Sample A-2 was reduced to 0.80 μm by the leaching process.

b. Particle Size Reduction

Sample A-2 was split into five batches, one 800-gm batch and four 650-gm batches. The 800-gm batch (Sample A-3) was slurried with 1350 cc of distilled water and milled with alumina balls in a one-gallon polyethylene jar for 100 hours. Nine 20 cc samples were periodically withdrawn during milling (Samples A-3-1 to A-3-9). Surface area and equivalent spherical particle size for each sample represent the extent of particle size reduction, Table V. The particle size dependence on ball-milling time, Fig. 6, provided the control necessary to achieve a specific particle size. X-ray investigation showed a detectable quantity of alumina after 52.3 hours with the alumina content increasing with time. To minimize contamination from mill balls, samples for ultraviolet degradation were limited to a maximum milling time of 36 hours.

Table V. Surface Areas and Particle Size of Zn_2TiO_4 Pigments

A-1	Surface Area[a] (m^2/gm)	Particle Size[a] μm	Comment
A-1	1.26	0.91	Reacted at 950°C
A-2	1.41	0.80	Acid Leached[b]
A-3-1	1.47	0.77	0.5 hr mill[c]
A-3-2	1.54	0.73	1.5 hr mill[c]
A-3-3	1.73	0.66	5.0 hr mill[c]
A-3-4	1.88	0.60	10.0 hr mill[c]
A-3-5	2.09	0.54	27.7 hr mill[c]
A-3-6	2.62	0.43	52.3 hr mill[c]
A-3-7	3.24	0.35	73.8 hr mill[c]
A-3-8	3.45	0.33	97.3 hr mill[c]
A-3-9	3.70	0.31	100.0 hr mill[c]

[a] Measurement of surface area and calculation of particle size has been described previously.[86]
[b] Reacted at 950°C prior to acid leach.
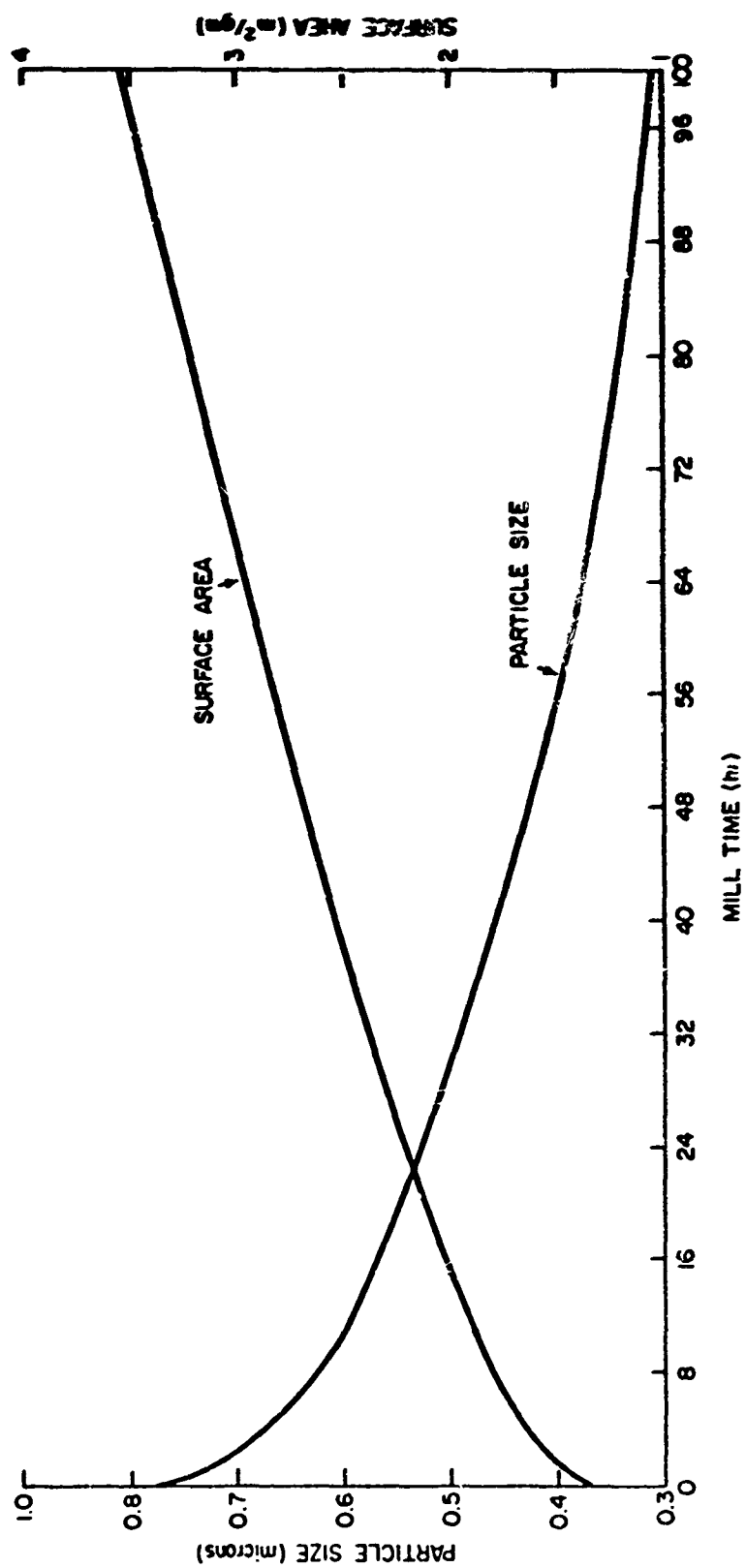[c] Reacted at 950°C and acid leached prior to ball milling.

26

Figure 6. Relationship between Particle Size and Bell Milling Time

27

Three of the four 650-gram batches, Samples A-4 to A-6, were slurried with 1050 cc of distilled water and ball-milled for 36.8 and 2 hours, respectively. Resultant equivalent particle sizes were 0.44, 0.58, and 0.61 μm for Samples 4, 5, and 6, respectively. The fourth batch, Sample A-7, was not ball-milled and had the same particle size as Sample A-2, 0.80 μm. All samples were dried at 110°C and crushed to 60 mesh.

c. Heat Treatment

Samples A-4 to A-7 were split into five 125-gram batches for heat treatment. Four batches from each sample were quench heated to 850, 950, 1050, and 1150°C, held for one hour, and quench cooled in 500 cc of distilled water. The fifth batch was quench heated to 850°C, held for one hour, and annealed to room temperature over three days, Fig. 7. All batches were fired as uncompacted powders in platinum cruci- bles. Temperature was controlled to ± 5°C in a silicon carbide resis- tance furnace. Each heat-treated batch was dried and ball-milled with 200 cc of distilled water for two hours. Twenty cc of each slurry were dried for surface area determinations.

d. Irradiation Powder Samples

Water slurries of twenty heat-treated pigments were sprayed onto heated aluminum substrates, 2.4-cm diameter by 0.08 cm thick. Multiple layers were applied under a dry nitrogen pressure of 16 psi. Two coated substrates of each sample were delivered to Mr. C. P. Boebel, Elastomers and Coatings Branch, Air Force Materials Laboratory, on August 25, 1971.

e. In Situ Reflectance

Ultraviolet exposure testing of the 20 Zn_2TiO_4 samples was accomplished in the equipment described in Section III.4.a. In situ pretest reflectance was measured in air and in a vacuum (4×10^{-6} torr). Reflectance was recorded at 18, 45, 110, and 230 equivalent ultraviolet sun hours. A final reflectance scan was made after 48 hours air expo- sure in the dark. Temperature of the specimen back was 49°C during irradiation.
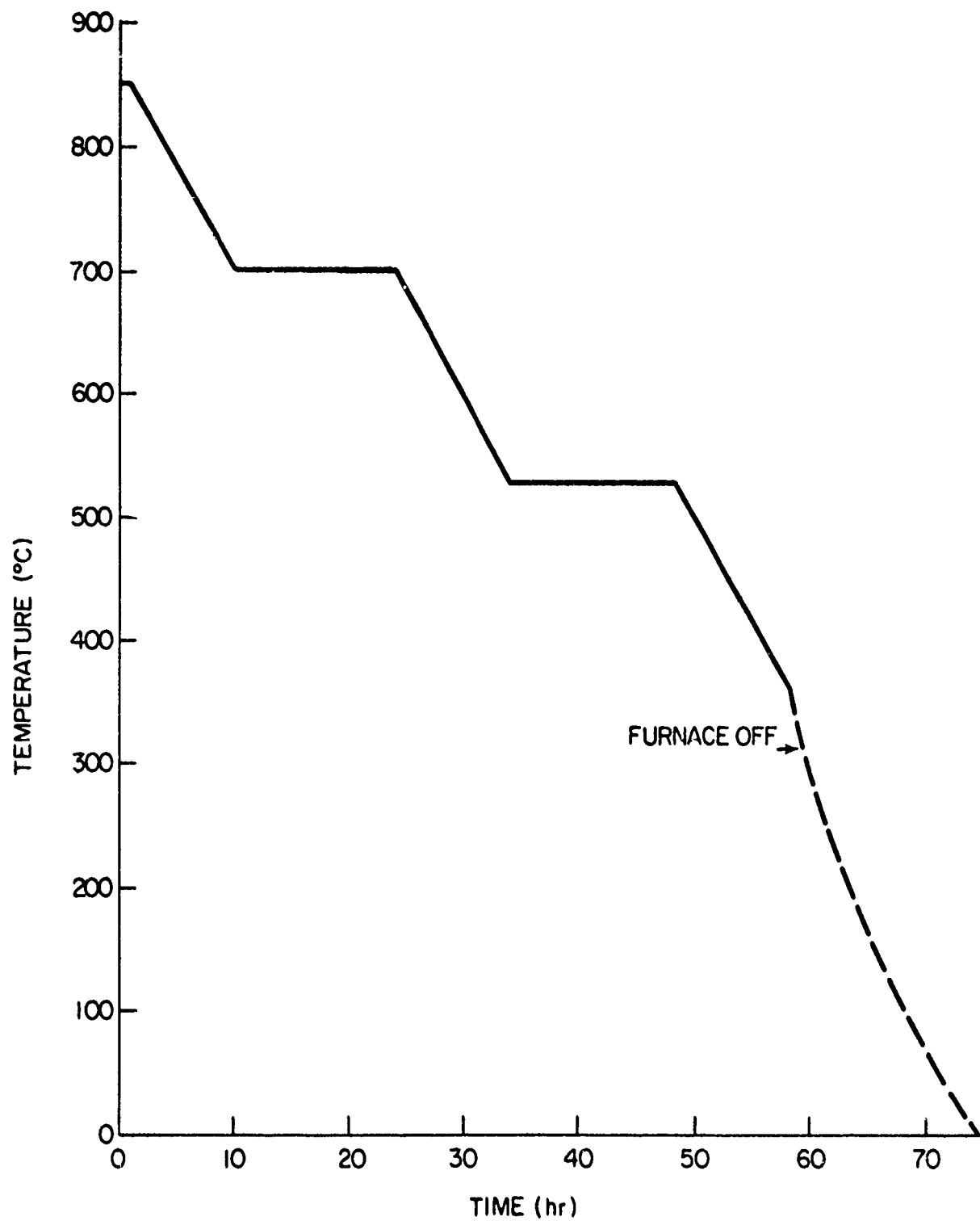
Figure 7. Annealing Curve for Zinc Orthotitanate Powders

IV. RESULTS AND DISCUSSION

1. Oxygen Transport

Oxygen transport properties of polydimethylsiloxane/rutile compositions were reported in AFML-TR-71-42, Part I.[88] For comparison with polymonomethylsiloxane properties, a portion of the polydimethylsiloxane data has been reproduced.

a. Polymethylsiloxanes

Oxygen sorption isotherms at 25°C for PDMS and PMMS, Fig. 8, show that Henry's law held for the pressure range investigated. Constant oxygen diffusion coefficients of $18.9 \pm 0.3 \times 10^{-6}$ and $5.02 \pm 0.09 \times 10^{-7}$ cm^2/sec at 25°C for PDMS and PMMS, respectively, for the pressure range 0 to 60 cm Hg established that diffusion coefficients were independent of concentration.

Oxygen transport properties in the polymethylsiloxanes are shown in Table VI. Permeability and diffusion coefficients of PDMS were an order of magnitude greater than values for PMMS and the solubility of PDMS was approximately 30 per cent lower. The lower diffusion coefficients in PMMS resulted from greater crosslinking and a lower methyl group concentration.

The temperature dependence of oxygen transport constants in the siloxanes conformed to the Arrhenius relationship within limits of experimental precision, Figs. 9-11. Least-squares activation energy for diffusion, Table VII, was 1300 cal/mole greater for the monomethylsiloxane and is attributed to the greater crosslinking in PMMS which limits chain flexibility. Permeability values and temperature dependence in both silicones were controlled by diffusion properties because solubility values and temperature dependence were similar.

b. Effect of Pigmentation

Temperature Dependence--After complete polymer curing, the temperature dependence of oxygen transport in the pigmented polymonomethylsiloxanes was exponentially related to temperature by the Arrhenius relationship within limits of experimental precision, Figs. 12-14. The least-square temperature coefficients are presented in Table VIII.

Solubility in PMMS Compositions--Where there are no voids and the polymer wets the pigment to the exclusion of gas adsorption, the solubility of the composite will be represented by

$$S = V_B S_B \qquad (33)$$

Preceding page blank
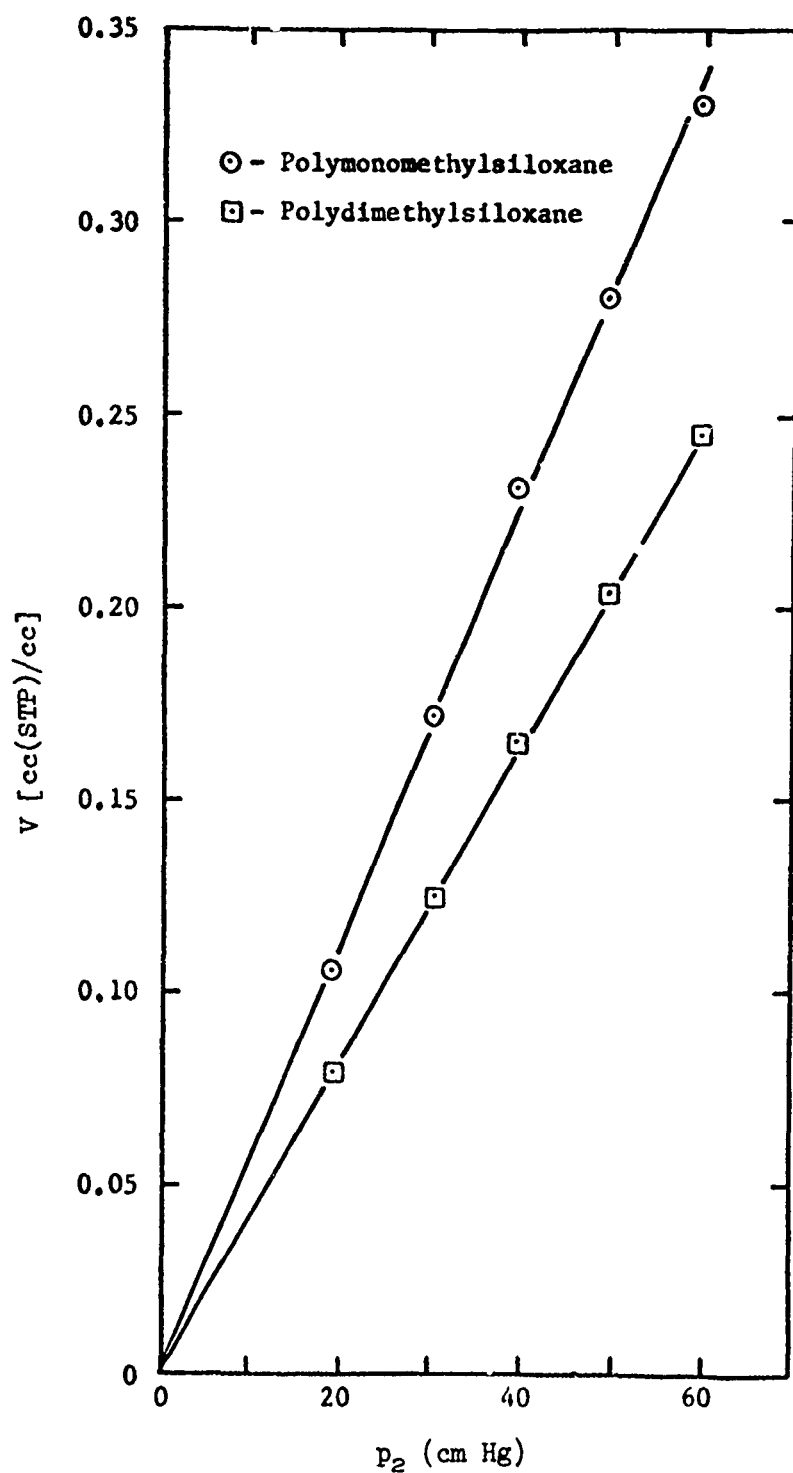
Figure 8. Oxygen Sorption Isotherms at 25°C

32

Table VI. Oxygen Transport in Polymethylsiloxanes

T (°C)	P (cc(STP)/sec/cm²/cm/cm Hg)	D (cm²/sec)	S (cc(STP)/cc/atm)
PDMS[a]			
0	5.28×10^{-8}	12.8×10^{-6}	0.313
25	7.41	19.1	0.294
32	8.06	21.1	0.289
42	9.04	24.2	0.283
50	9.86	26.8	0.278
PMMS			
0	1.68×10^{-9}	2.68×10^{-7}	0.476
25	2.83	5.02	0.428
32	3.29	5.55	0.450
50	4.72	7.92	0.453
60	5.95	10.2	0.443

[a]Least-squares values for average of three samples.
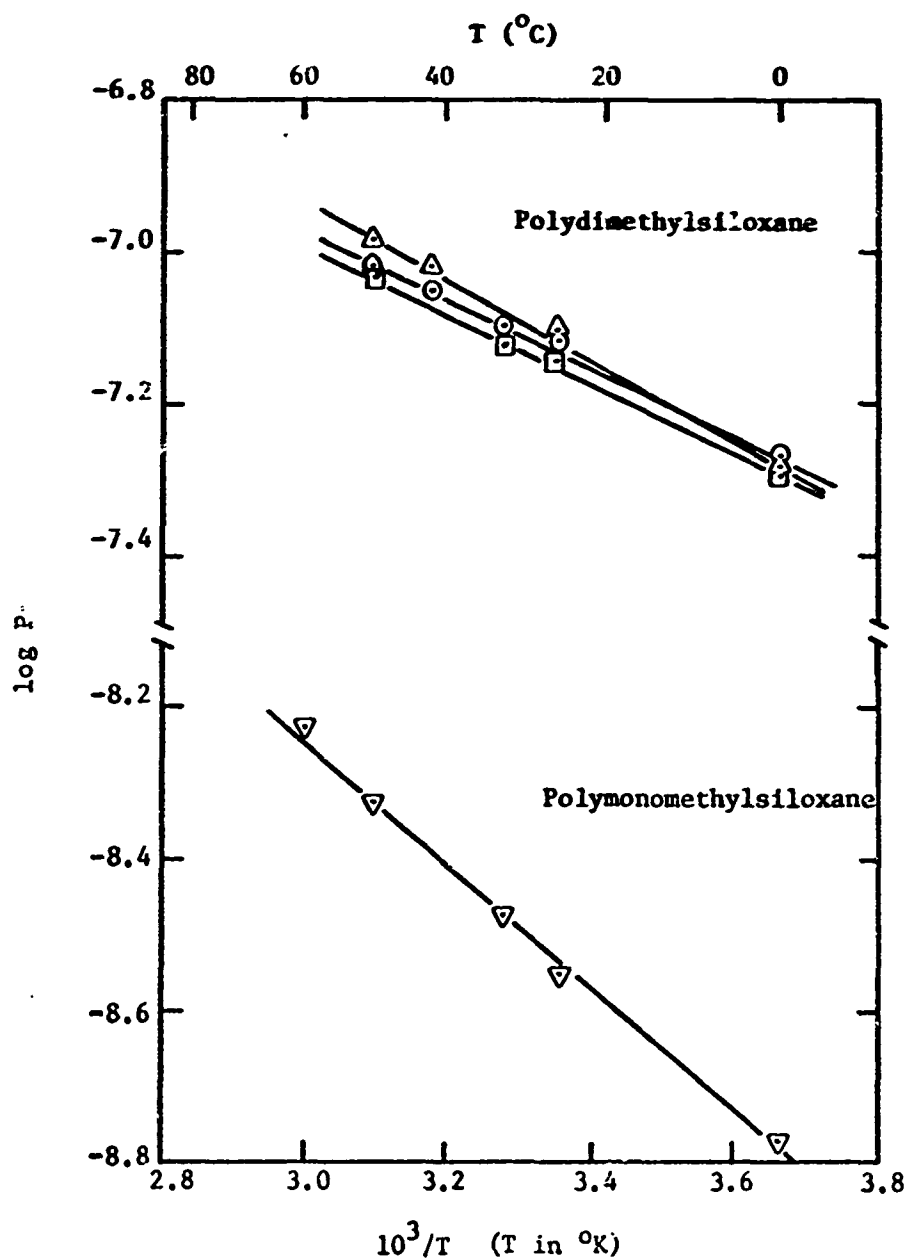
Figure 9. Temperature Dependence of Permeability Constants for Oxygen in Polymethylsiloxanes
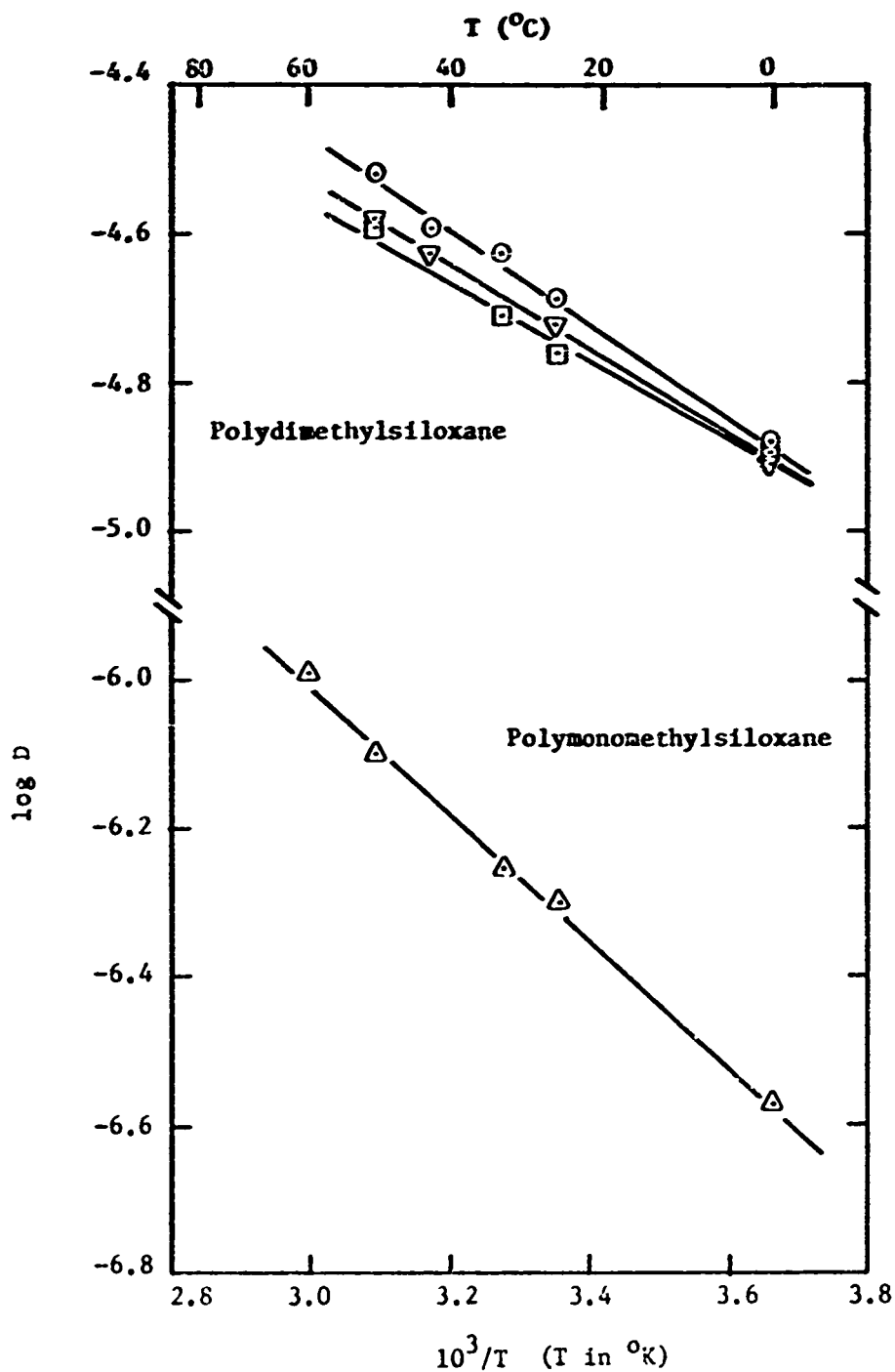
Figure 10. Temperature Dependence of Diffusion Coefficients for Oxygen in Polymethylsiloxane
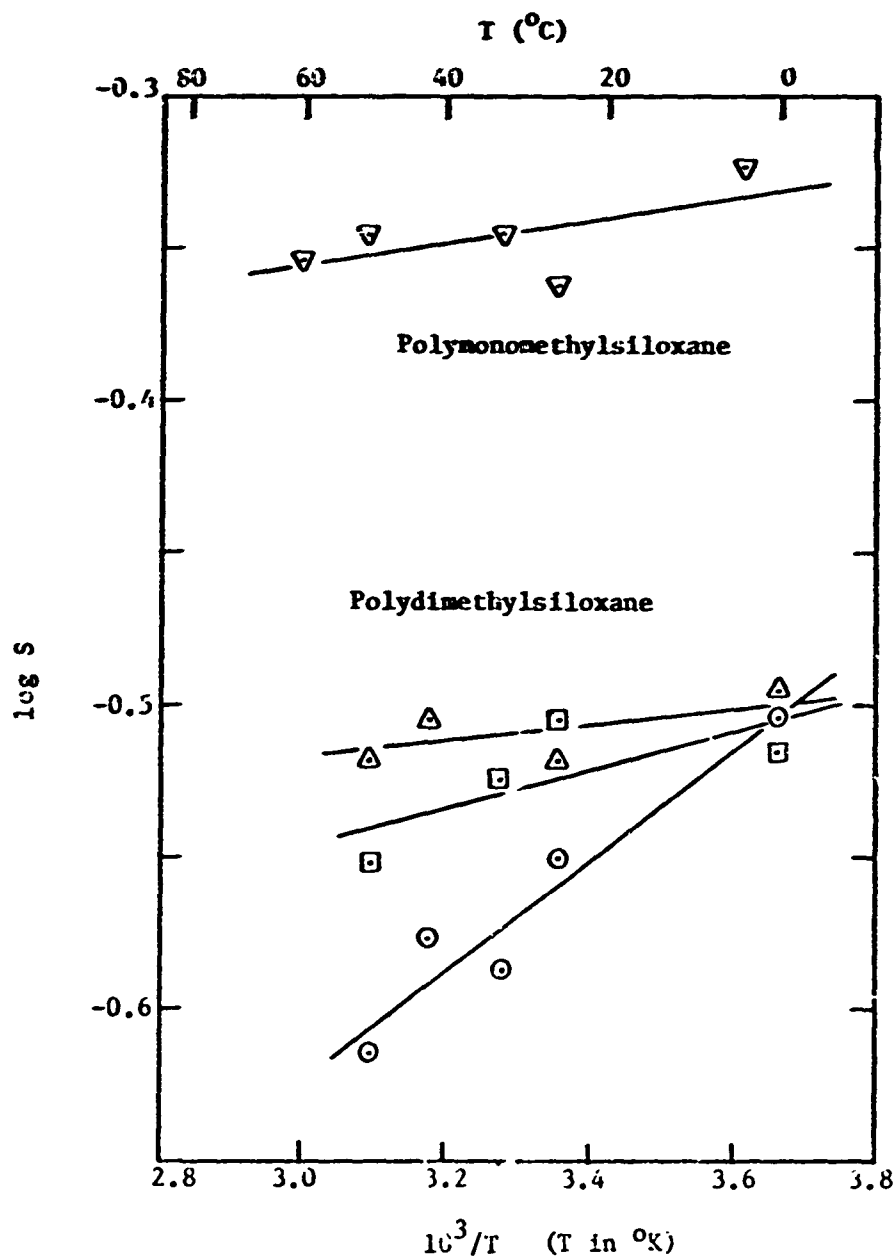
Figure 11. Temperature Dependence of Solubility Constants
for Oxygen in Polymethylsiloxanes

Table VII. Arrhenius Constants for Oxygen Transport in Polymethylsiloxane

Sample	P_0 (cc(STP)/sec/ cm^2/cm/cm Hg)	E_p (cal/mole)	Std. Error of E_p (cal/mole)
PDMS-1	2.25×10^{-6}	2019	67
PDMS-2	2.64	2138	99
PDMS-3	4.45	2407	107
PDMS-Ave.	2.98	2188	
PMS	1.71	3774	136

Sample	D_0 (cm^2/sec)	E_D (cal/mole)	Std. Error of E_D (cal/mole)
PDMS-1	2.46×10^{-3}	2837	140
PDMS-2	1.07	2418	207
PDMS-3	1.39	2522	46
PDMS-Ave.	1.54	2602	
PMS	0.38	3936	150

Sample	S_0 (cc(STP)cc/atm)	ΔH_s (cal/mole)	Std. Error of Δ_s (cal/mole)
PDMS-1	0.068	-829	145
PDMS-2	0.186	-280	208
PDMS-3	0.247	-134	100
PDMS-Ave.	0.247	-414	
PMS	0.346	-159	145
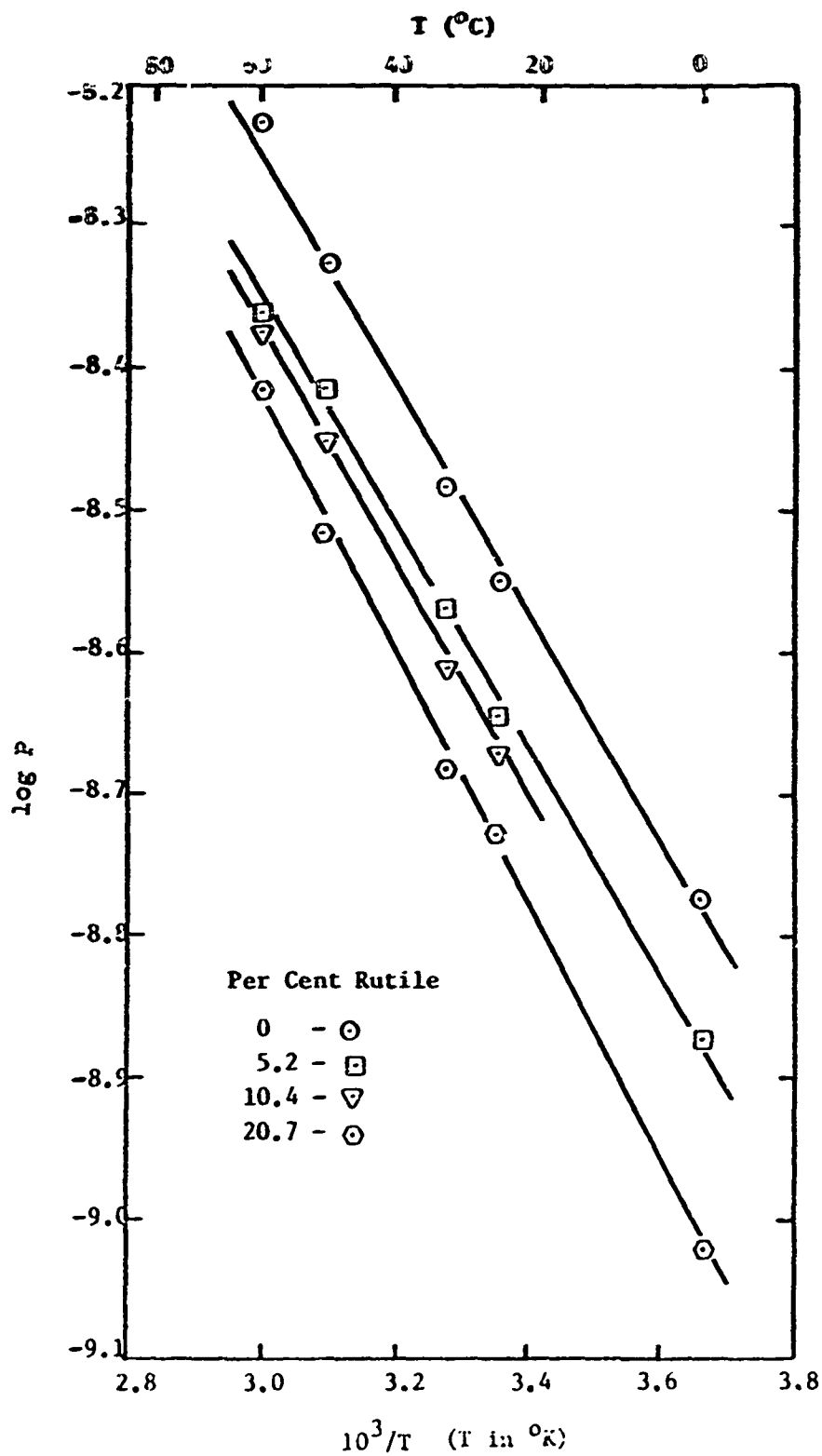
Figure 12. Temperature Dependence of Permeability Constants
for Polymonomethylsiloxane/Rutile Compositions

38
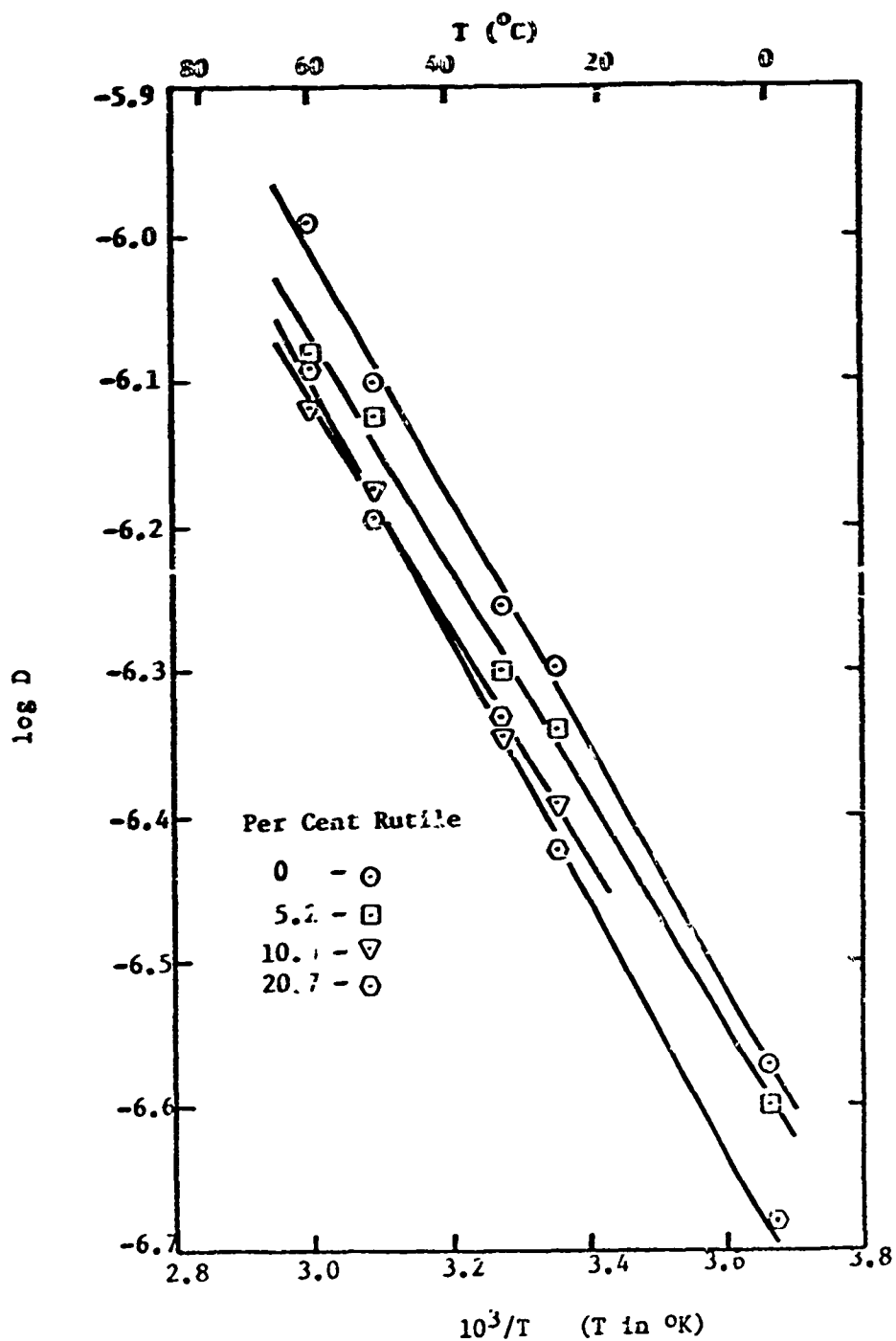
Figure 13. Temperature Dependence of Diffusion Coefficients for Oxygen in Polymonomethylsiloxane/Rutile Compositions

39
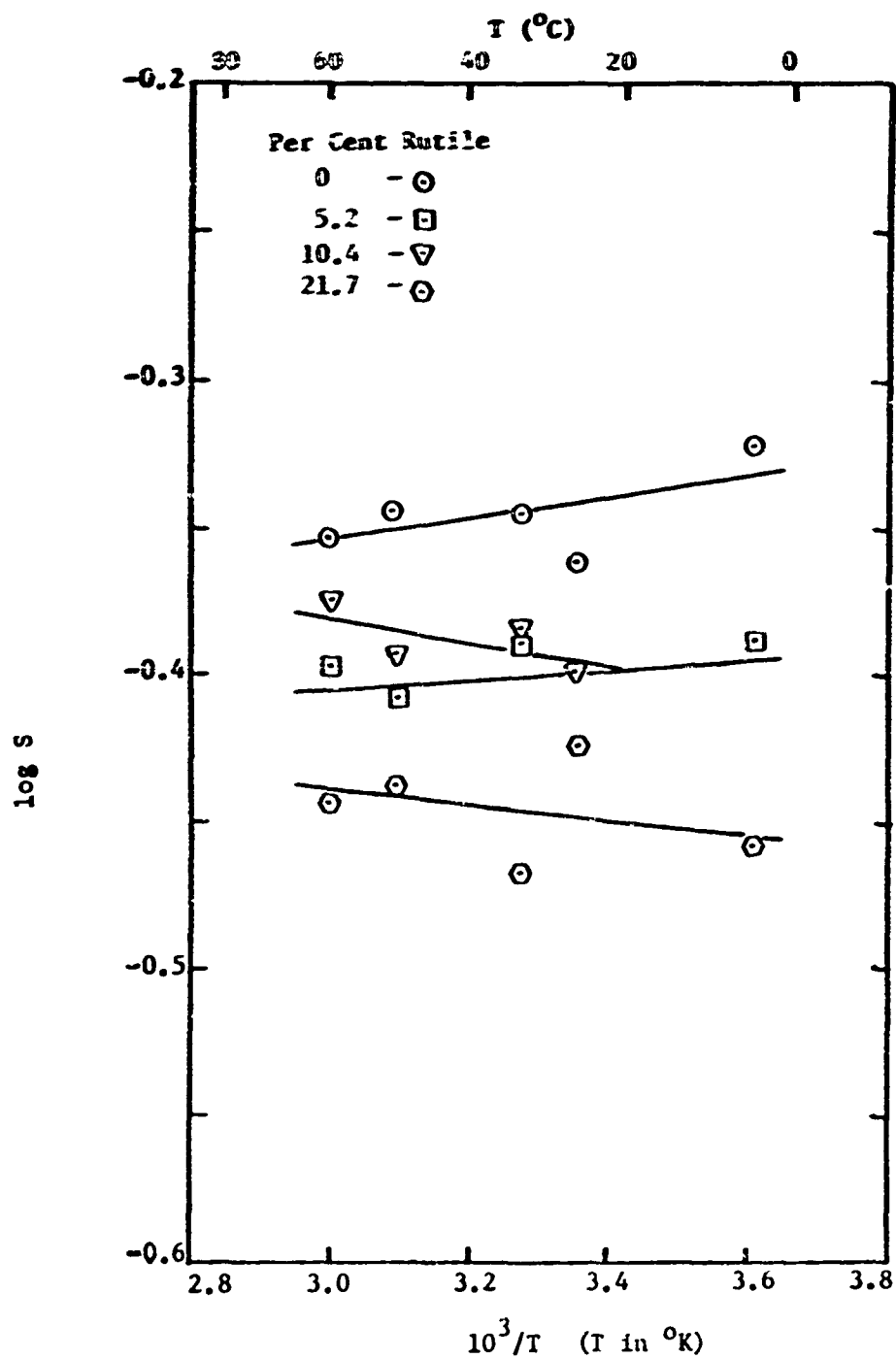
Figure 14. Temperature Dependence of Solubility Constants for Oxygen in Polymonomethylsiloxane/Rutile Compositions

Table VIII. Arrhenius Constants for Oxygen in Polymono-Methylsiloxane/Rutile

Sample	$P_0 \times 10^6$ cc(STP)/sec/ $(cm^2/cm/cm\ Hg)$	E_p (cal/mole)	Std. Error of E_p (cal/mole)
10	1.71	3774	136
11	1.06	3624	109
12	1.47	3874	108
13	1.96	4136	116

Sample	$D_0 \times 10^4$ (cm^2/sec)	E_D (cal/mole)	Std. Error of E_D (cal/mole)
10	3.77	3936	150
11	2.24	3685	154
12	2.05	3694	202
13	3.57	4043	124

Sample	S_0 (cc(STP)/ cc/atm)	ΔH_S (cal/mole)	Std. Error of ΔH_S (cal/mole)
10	0.346	-159	145
11	0.359	-60	153
12	0.560	197	145
13	0.417	94	169

where V_B is the volume fraction of the polymer and S_B is the solubility constant of the polymer.[38] There was no indication of oxygen adsorption on rutile in the PMMS compositions. The concentration dependence of the solubility constants was well represented by equation (33), dashed lines in Fig. 15. Scatter in solubility values was greater than found in PDMS compositions due to the variations in PMMS membranes. Comparison of observed and calculated densities indicated negligible porosity. Heats of solution were constant within limits of experimental precision for all rutile concentrations, Table 8.

Adsorption on the rutile may occur in PMMS compositions since it is common for PDMS compositions above 20 per cent. A PMMS composition with 30 per cent rutile was investigated but oxygen flow through the membrane was too rapid for determination of permeability and diffusion. Thermal expansion mismatch between the brittle PMMS and rutile resulted in fine cracks after thermal curing. Critic acid additions increased membrane flexibility but the samples remained very brittle and required careful handling.

Permeability in PMMS Compositions--Permeability in a heterogeneous medium such as a pigmented polymer may be described by

$$P = K\ V_B P_B;$$
(34)

where K is a structure factor and P is the permeability constant of the polymer. Rayleigh's structure factor for a cubic lattice of spheres was used to explain the pigment concentration dependence of permeability constants. Values of K were reported in AFML-TR-71-42, Pt. 1.[88]

Permeability constants for PMMS compositions decreased with increasing pigment concentration; however, permeability values were lower than predicted by equation (34), Fig. 16. Considering the excellent agreement for PDMS compositions formulated with the same pigment, the discrepancy is most likely caused by thickness variation of the PMMS membranes. There is no reason to think that permeability constants for pigment-free PMMS are more accurate than for pigmented compositions, and it is probable that pigment-free constants were high.

Diffusion in PMMS Compositions--Diffusion coefficients decreased as pigmentation increased, Fig. 17. These data were compared to values predicted by Rayleigh's structure factor for the case of a nonadsorbing filler

$$D = K\ D_B$$
(35)

where D_B is the diffusion coefficient of the polymer. Diffusion coefficients were lower than predicted by equation (35). This may result by either sorption on the pigment or thickness variation. Thickness variations will cause the permeability and diffusion constants of a
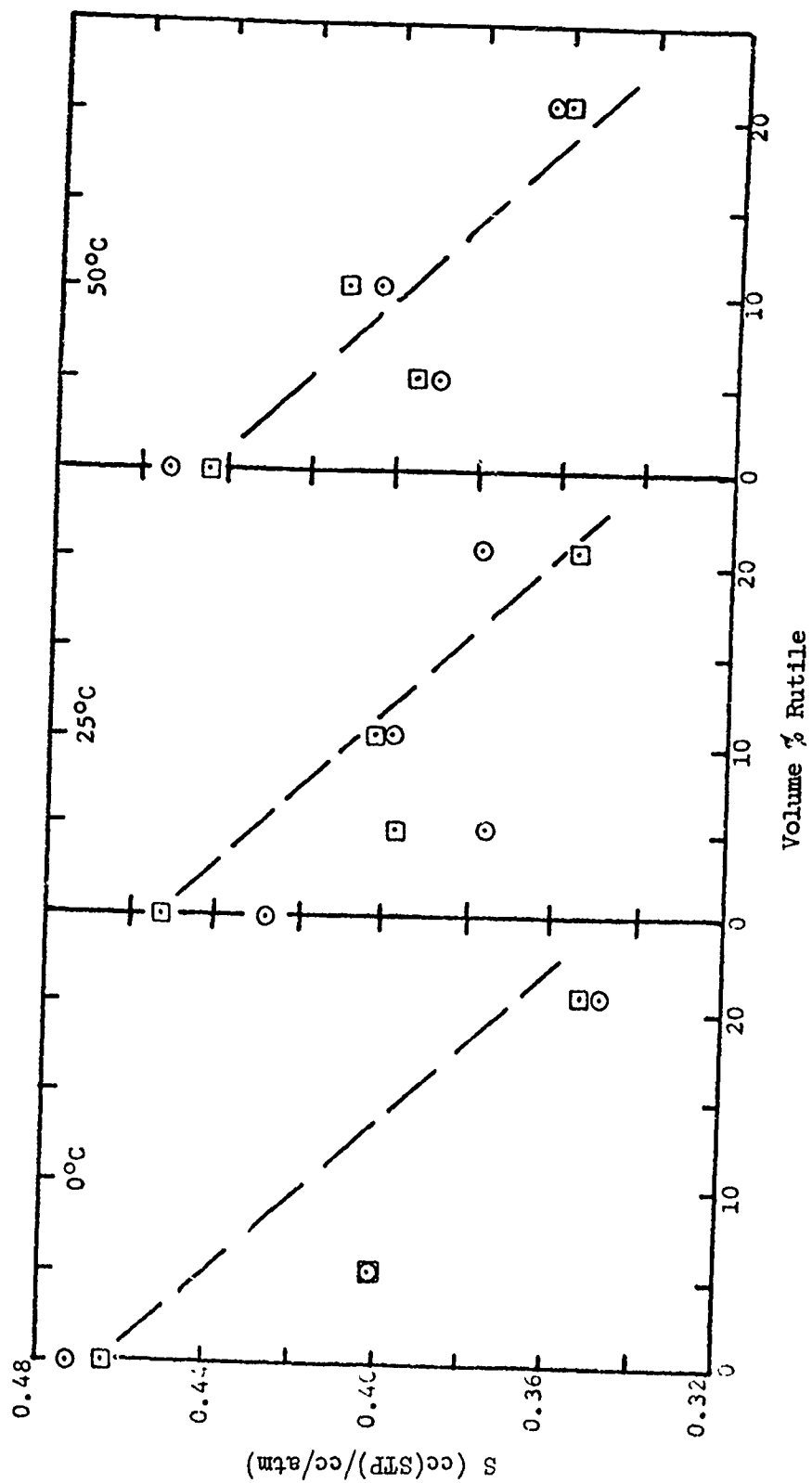
Figure 15. Effect of Pigmentation on Oxygen Solubility in Polymonomethylsiloxane.
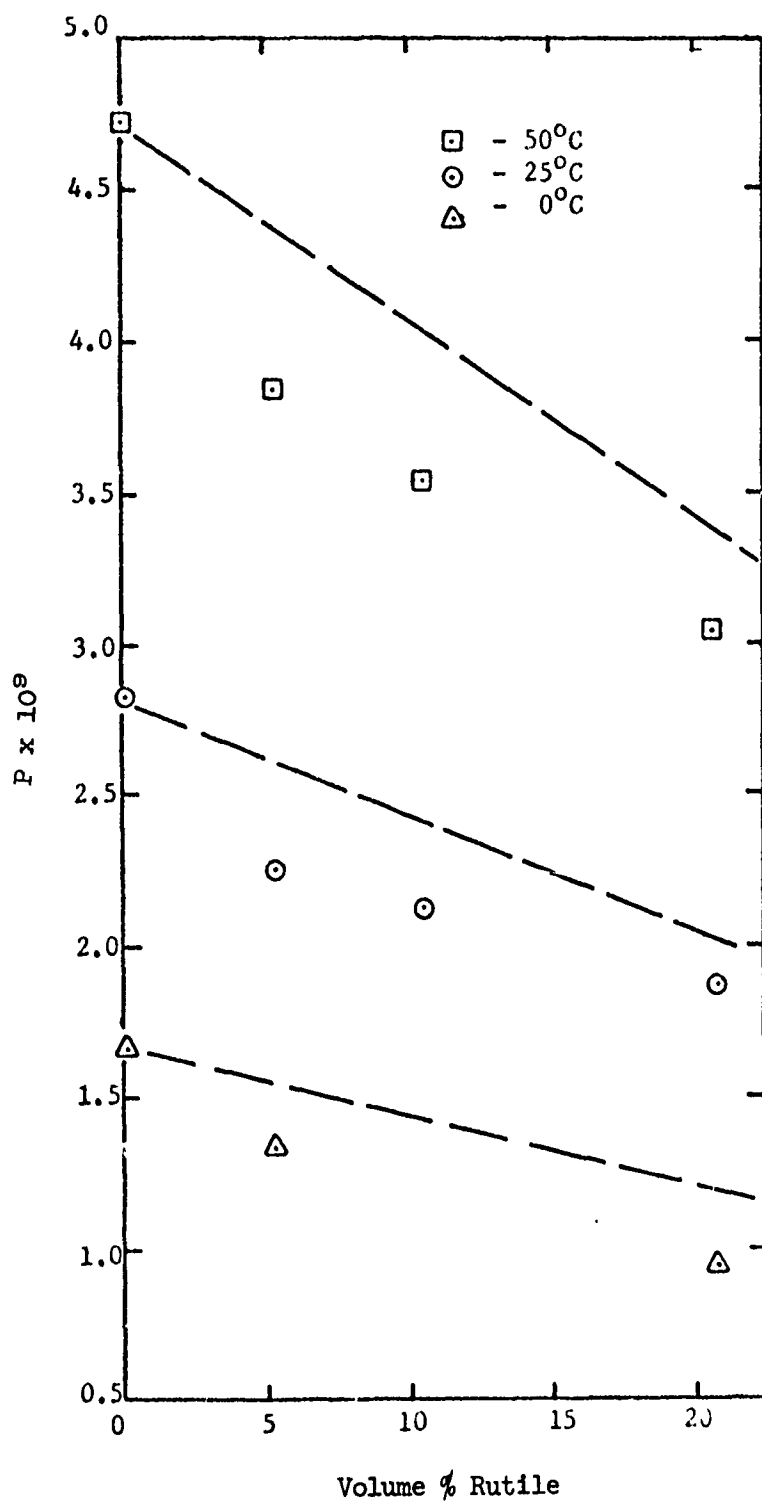⊙- Observed Values, ⊡- Least-Squares Values

43

Figure 16. Effect of Pigmentation on Oxygen Permeability in Polymonomethylsiloxane. Dashed lines are equation (34)
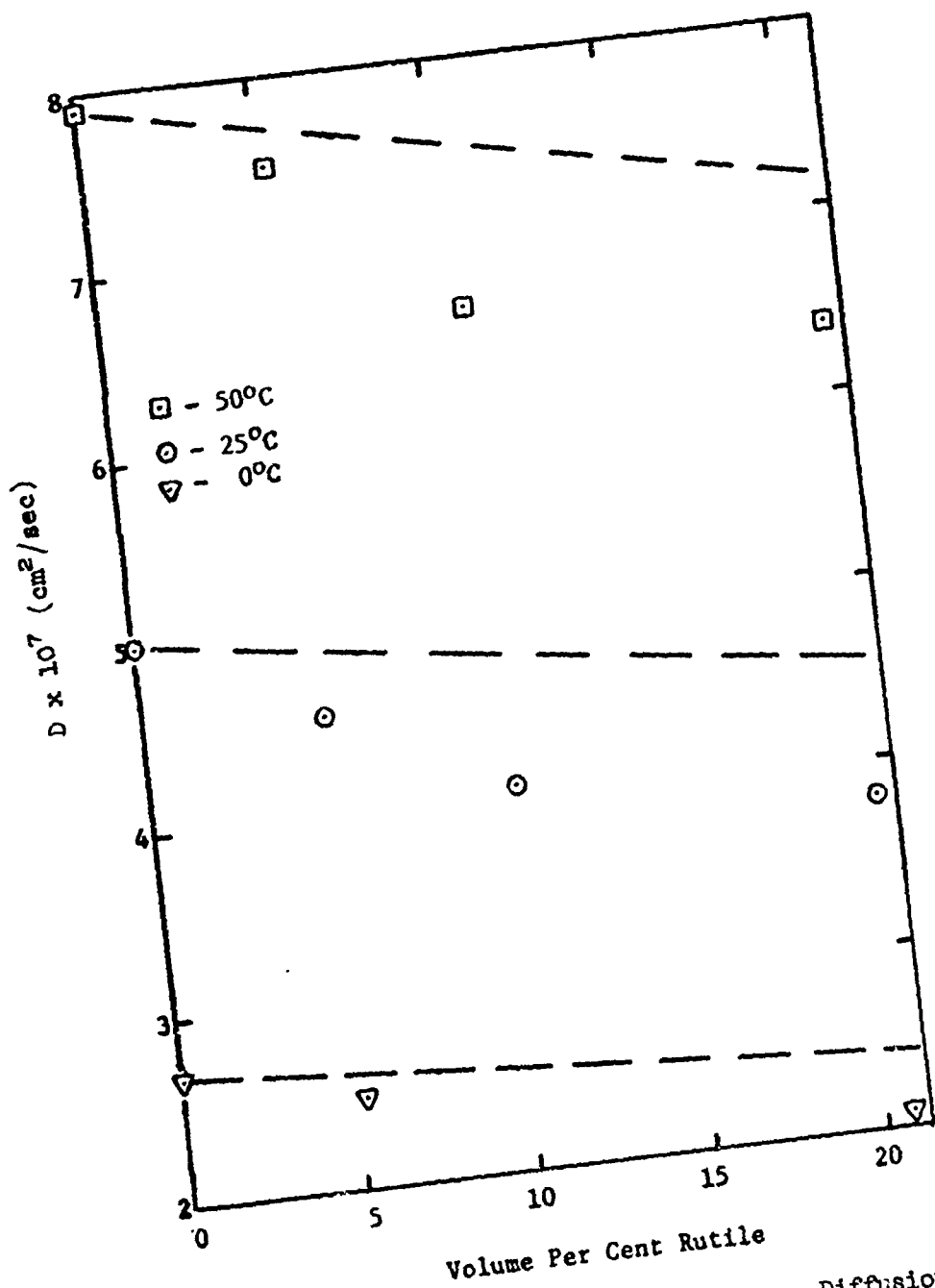
Figure 17. Effect of Pigmentation on Oxygen Diffusion in Polymonomethylsiloxane. Dashed lines are equation (35)

45

sample to deviate consistently from predicted values. Comparison of Figs. 16 and 17 show this. Thus, there is no basis for concluding oxygen sorption on the pigment in PMMS compositions.

2. Contact Angle

The reflections of normal and inverted water drops, Fig. 18, delineated water-solid interfaces except at angles near 90°. Contact angle differences due to gravity, $\Delta\theta_g$, were 1 to 4°. For example, the height to radius ratio, h/r, of a water drop on PDMS, Fig. 18, increased from 1.16 to 1.32 on the inversion but the contact angle decreased only 1°. Calculations of contact angles on PDMS, using the equation for spherical geometry,[89]

$$\tan \theta/2 = h/r, \qquad (36)$$

resulted in 98 and 106° for the normal and inverted positions, respectively, an average of 102° which agrees with the 101° measured average value. Gravity has a larger affect on drop shape than on contact angle; however, in all cases, inversion decreased contact angles, Table IX.

Table IX. Water Contact Angles

| Sample | Contact Angle | | | |
	Normal	Inverted	Average	$\Delta\theta_g$
Rutile - 1	42 ± 2	38 ± 3	40	3
Rutile - 2	29 ± 2	27 ± 4	28	2
PDMS	102 ± 3	101 ± 2	101	1
PMMS	90 ± 1	89 ± 1	90	1
PDMS/Rutile	92 ± 3	89 ± 2	90	3
PMMS/Rutile	80 ± 1	76 ± 1	78	4
Rutile/PDMS-1	80 ± 2	78 ± 1	79	3
Rutile/PDMS-2	73 ± 2	70 ± 3	72	3
Rutile/PMMS	61 ± 5	58 ± 4	60	3

46

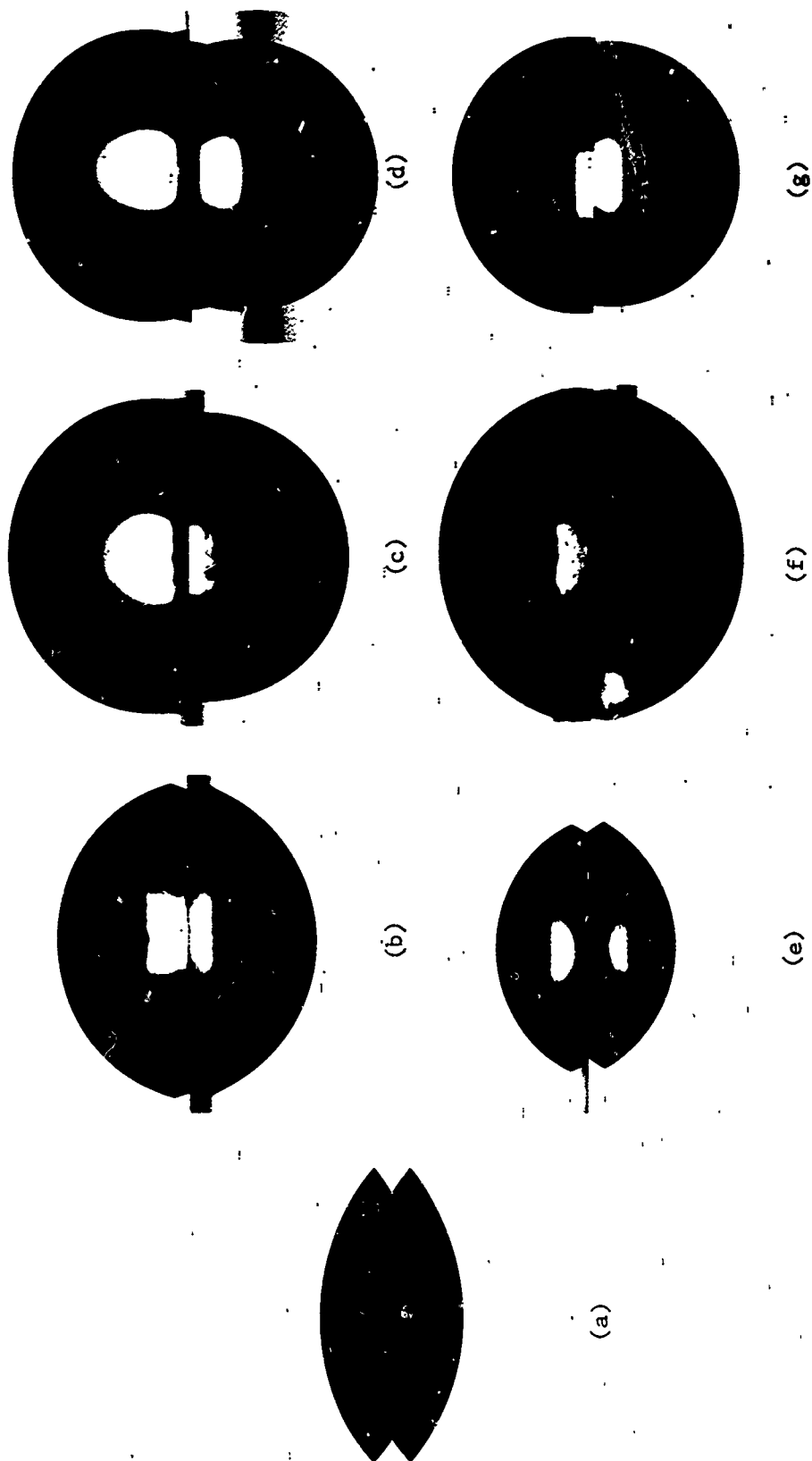Figure 18. Normal and Inverted Water Drop on (a) Rutile, (b) Rutile Separated from PDMS, (c) PDMS Separated from Rutile, (d) Free-Formed PDMS, (e) Rutile Separated from PMMS, (f) PMMS Separated from Rutile, and (g) Free-Formed PMMS

47

Complete wetting had been expected on rutile but average contact angles of 28 and 40° were observed. Scanning electron micrographs, Fig. 19, showed submicron scratches and a maximum pore diameter of 20 microns with the majority below 10 microns. Such microscopic roughness was too small to produce the high contact angles.[90] The surface consisted of rutile and a glassy phase which occupied 21 per cent of the surface, Fig. 19. The contact angle of a composite may be calculated from[91]

$$\cos \theta_c = f_1 \cos \theta_1 + f_2 \cos \theta_2 \qquad (37)$$

where θ_c, θ_1, and θ_2 are the contact angles of the composite, phase 1 and phase 2, respectively, and f_1 and f_2 are surface fractions. Both rutile and glass should be completely wet by water and θ_c should be zero. Strain can increase water contact angles on glass to 80° and may account for the high contact angles.[92]

The average contact angle of 101° for PDMS agreed with Shafrin and Zisman.[93] A lower methyl group surface concentration in PMMS resulted in a lower contact angle of 90°. Curing polymethylsiloxanes on rutile resulted in contact angles 11 and 12° lower than angles on free-formed surfaces. Using Moser's hypothesis,[94] both results predicted better adhesion for PMMS than for PDMS. The ease of stripping the siloxanes from rutile showed the adhesion to be small.

Rutile surfaces separated from cured siloxanes have high contact angles. The increase may have resulted from incomplete solvent removal and/or a residue of methyl groups.

3. Silicone/Rutile Optical Properties

a. Solar Reflectance

The reflectance spectra for the water sprayed rutile, PDMS/20 per cent rutile, and PMMS/20 per cent rutile are shown in Figs. 20 through 22. Reflectance of the paints was higher in the visible and lower in the infrared than for rutile powder. Characteristic silicone absorption lowered infrared reflectance, and specular reflection from the smooth silicone surfaces increased visible reflectance. The lower refractive index of PDMS caused a larger relative refractive index for PDMS/rutile paints. The initial solar reflectance of PDMS paints exceeded PMMS paints, Fig. 23. Solar reflectance maximized between 10 and 20 per cent rutile. Increased scattering from low pigment concentrations were offset by loss of surface gloss at higher pigment concentrations.
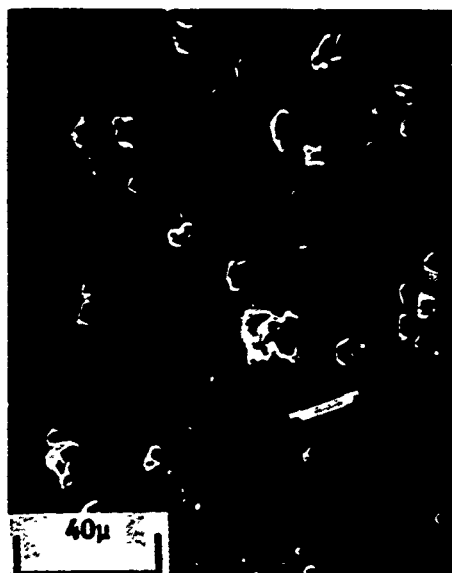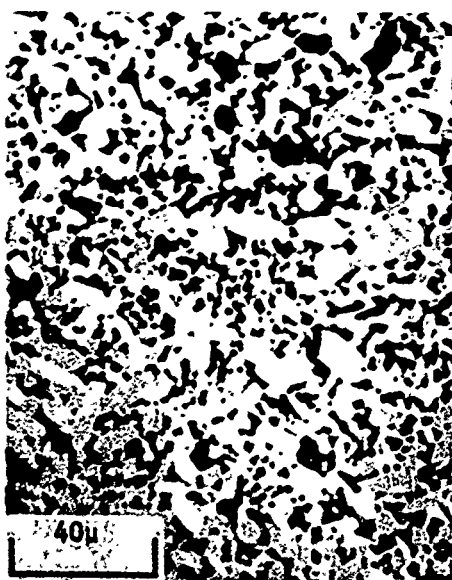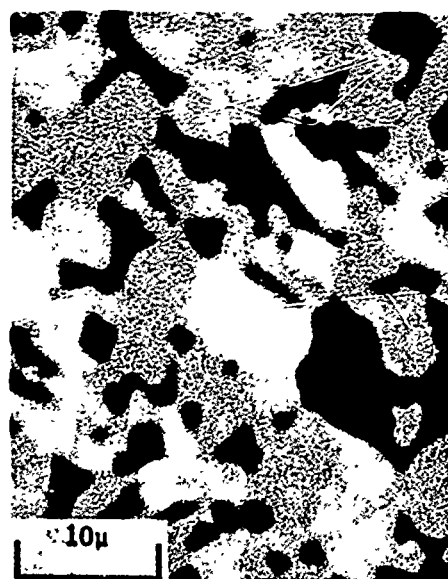
Figure 19. Polished Rutile: (a) and (b), Scanning Electron Micrographs, 500X and 2000X, Respectively; (c) and (d), Reflected Light Micrographs of Unetched Surface, 500X and 2000X, Respectively

49
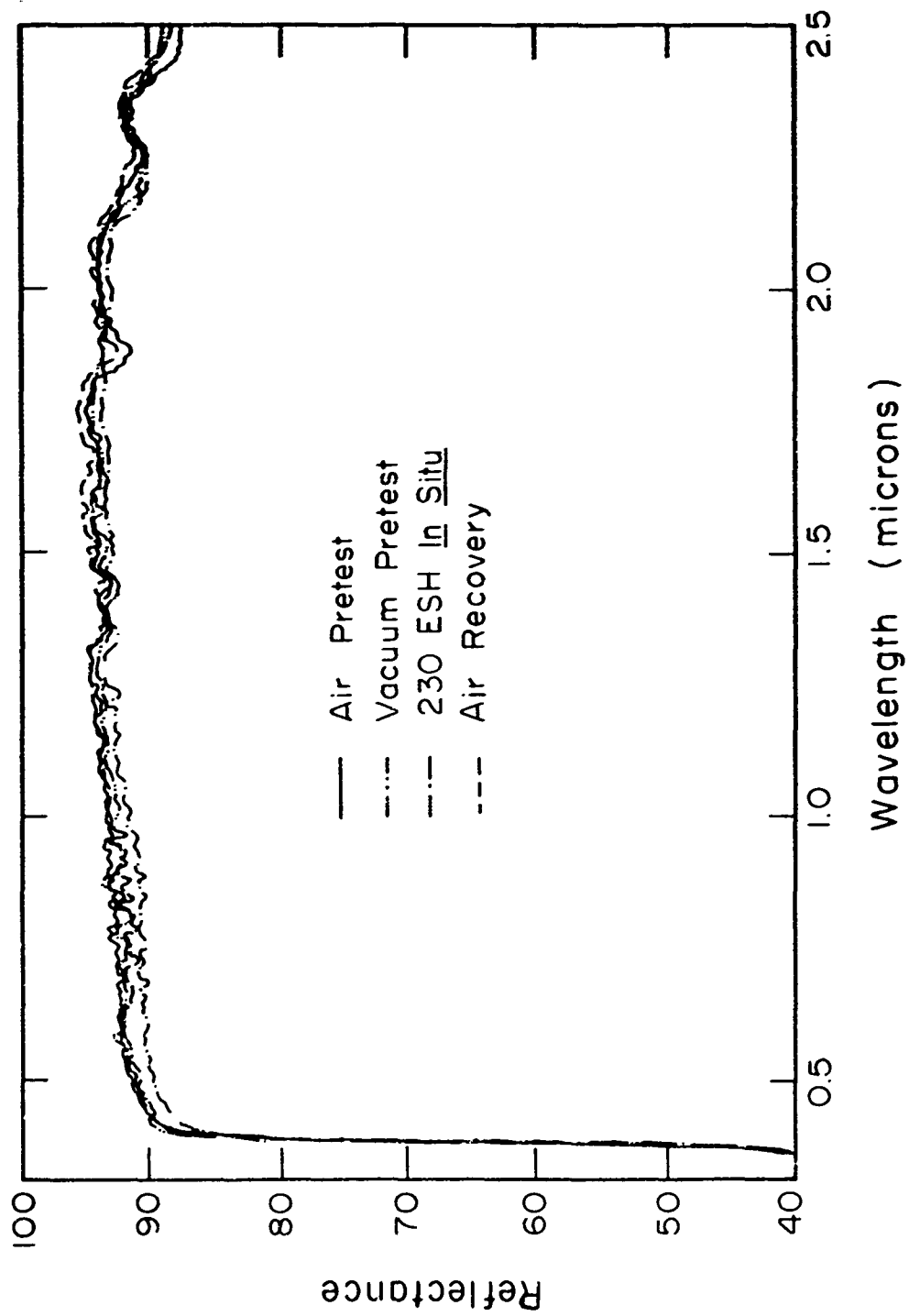
Figure 20. Reflectance Spectrum of Silicate-Coated Rutile
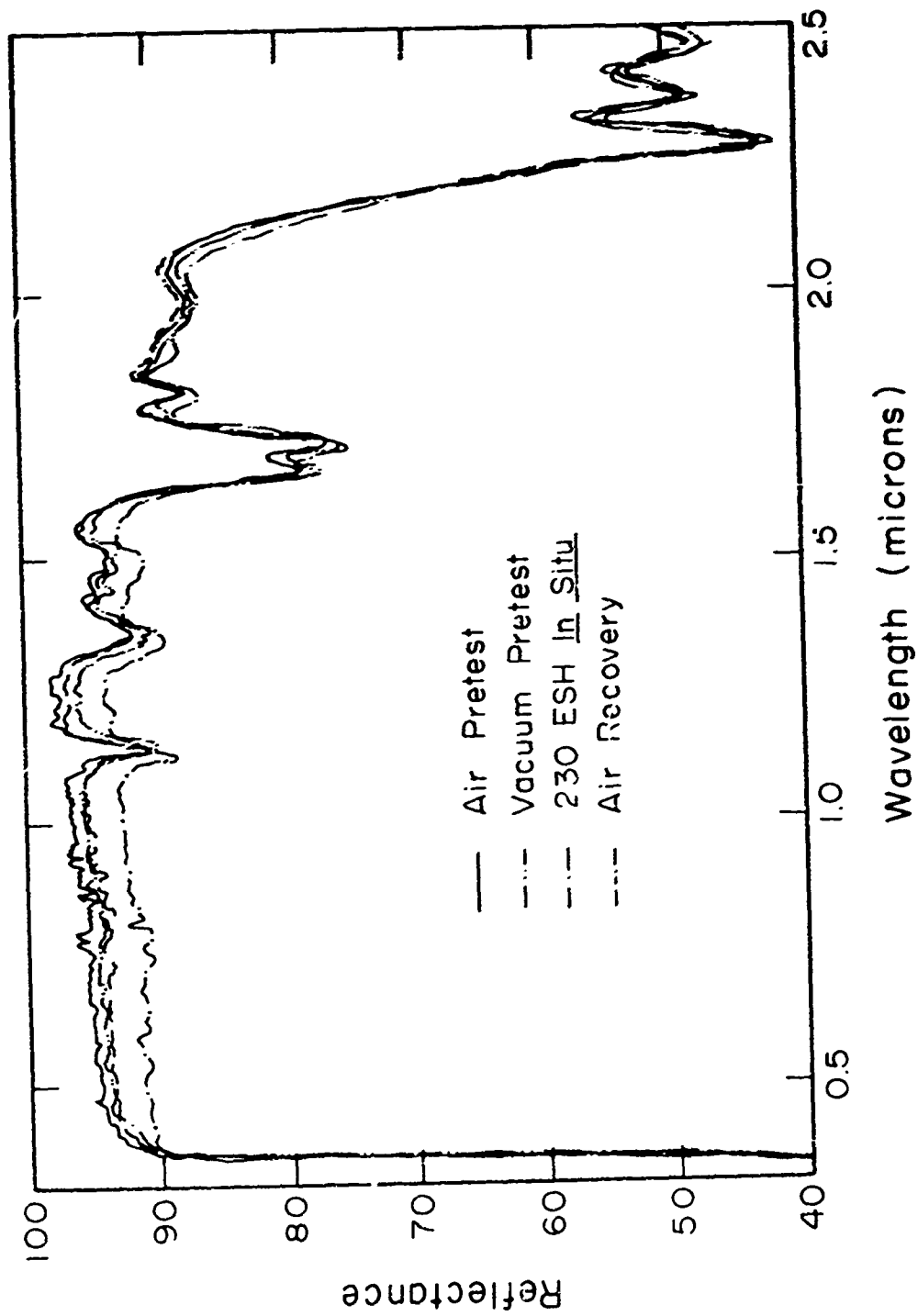
Figure 21. Reflectance Spectrum of Polydimethylsiloxane/20 Per Cent Rutile
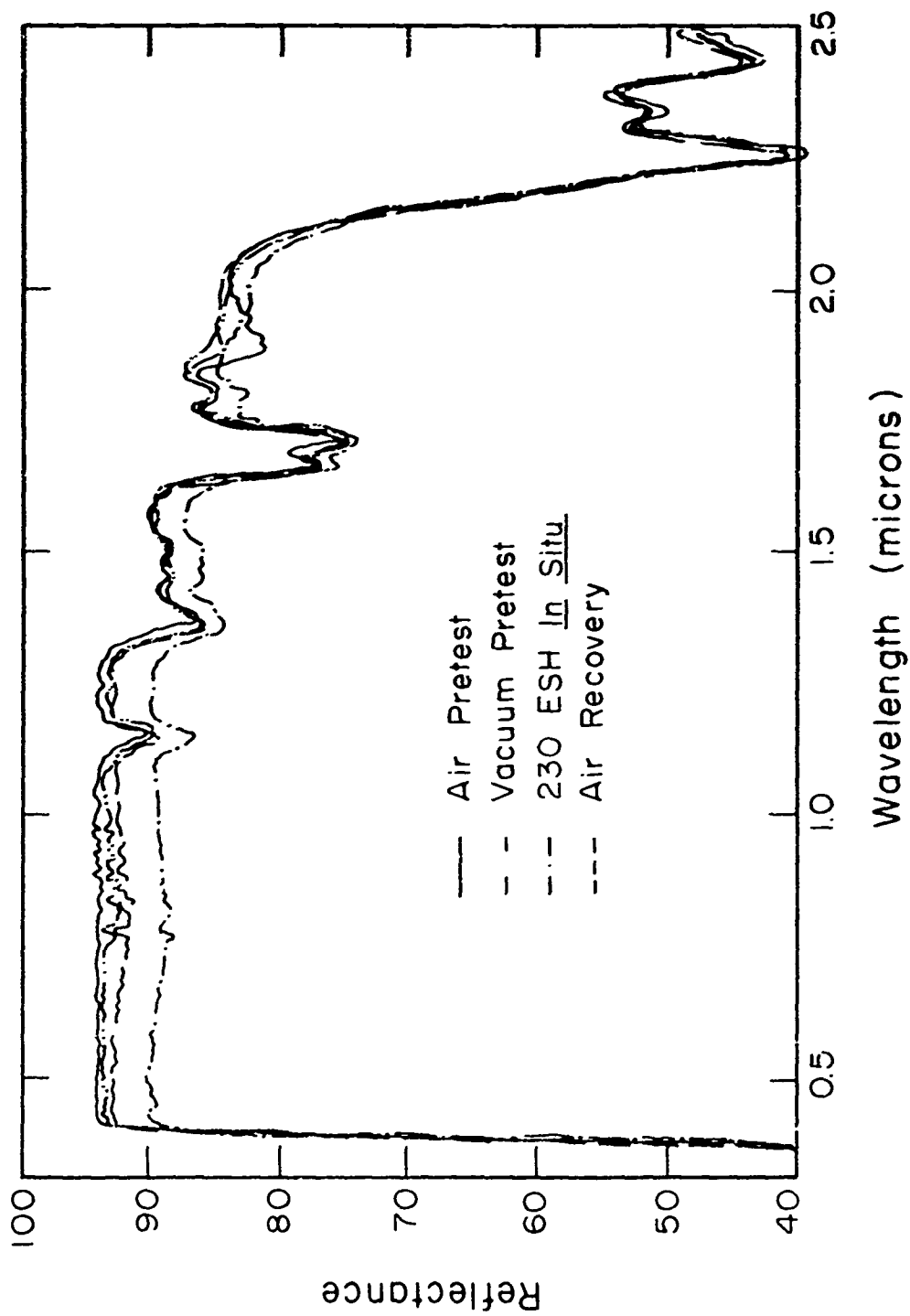
Figure 22. Reflectance Spectrum of Polymonomethylalloxane/20 Per Cent Rutil.
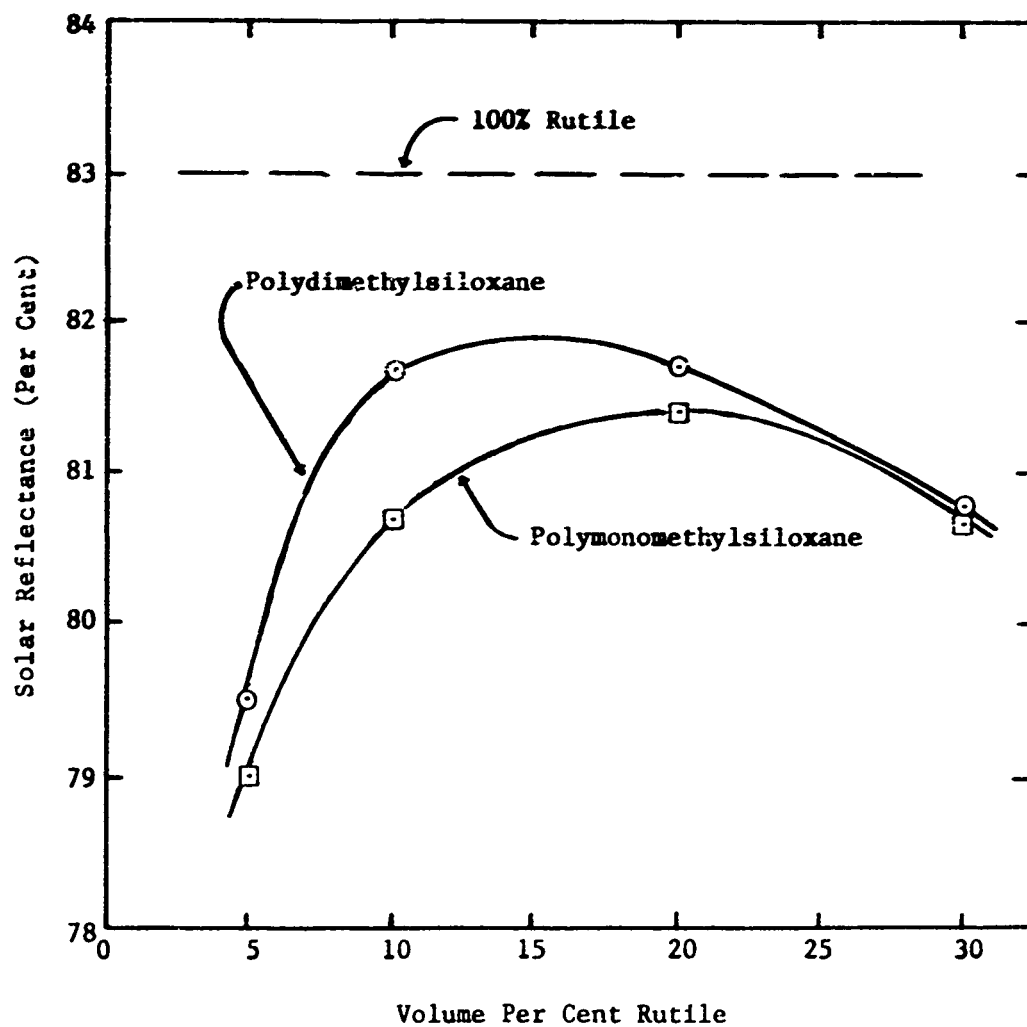
Figure 23. Effect of Pigment Concentration on Solar Reflectance
of Rutile/Silicone Paints

53

b. **Induced Solar Absorptance**

The stability of the silicate-coated rutile produced an induced absorptance of 0.009 in 230 ESH, Table X. Silicate coating produced degradation resistance similar to that of silicate-coated zinc oxide[95] and zinc orthotitanate[96] and was the first time the effect has been observed for rutile.

The recovery bleaching of rutile supported the oxygen dependence of the irradiation damage. Differences between induced absorptances at 230 ESH and air recovery values for the paints, Table X, were about equal to that of the binderless pigment. Bleaching was attributable to the pigment and permanent damage represented polymer degradation. Silicone permeability was too high to produce observable differences in pigment degradation.

Induced solar absorptance of PMMS paints was constant, Fig. 24, and indicated equal degradation from PMMS and rutile. For PDMS paints, induced solar absorptances in the pigment increased with concentration increases to 20 per cent and continued to decrease to 30 per cent.

The pigment degraded approximately the same in both PDMS and PMMS. Thus, surface interaction between the pigment and the polymer did not measurably affect degradation.

Water associated with the pigment was indicated by the characteristic absorption band at 1.9μ which increased in intensity with increasing pigment concentration. For the PDMS series no absorption occurred for samples 1 (5% TiO_2) and 2 (10% TiO_2), slight absorption for sample 3 (20% TiO_2) and strong absorption for sample 4 (30% TiO_2). These results support the oxygen solubility data which indicated oxygen sorption on the pigment starting at 20 volume per cent and increasing with concentration.[97] In contrast to oxygen solubility data which did not show sorption on the pigment, PMMS paints had strong water desorption that increased with increasing pigment concentration. Citric acid, present in PMMS oxygen transport samples but not in UV irradiated paints, may have adsorbed on the pigment preventing oxygen sorption. Water absorption disappeared in vacuum and partially reappeared when returned to ambient conditions.

4. **Silicone/Zinc Oxide Degradation**

Infrared reflectance decreases of 4 to 10 per cent were observed between initial in-air scans and pre-irradiation vacuum scans for all samples. Characteristic water absorption was absent and the reflectance decreases demonstrate the extreme surface oxygen sensitivity of infrared spectrum of zinc oxide. Pre-irradiation vacuum solar absorptances and ultraviolet induced solar absorptance are reported in Table XI

54

Table X. Silicone/Rutile Solar Absorptances

Volume % Rutile	Solar Absorptance			$\Delta\alpha_s$		
	Vacuum Pretest	45 ESH	230 ESH	45 ESH	230 ESH	Air Recovery[a]
Polydimethylsiloxane/Rutile						
5	0.205	0.210	0.216	0.005	0.011	0.01
10	0.183	0.195	0.199	0.012	0.016	0.01
20	0.183	0.196	0.207	0.013	0.024	0.01
30	0.192	0.197	0.202	0.005	0.0⌢0	0.01
Polymonomethylsiloxane/Rutile						
5	0.210	0.224	0.236	0.014	0.026	0.02
10	0.193	0.207	0.227	0.014	0.034	0.02
20	0.186	0.199	0.214	0.013	0.028	0.02
30	0.193	0.205	0.221	0.012	0.028	0.02
Binderless Rutile	0.170	-	0.179	-	0.009	0.00

[a] These values are estimated and indicate the degree of permanent damage.

Note: The solar absorptance values shown to three places do not signify the accuracy of the reflectance measurement but merely relative degradation trends of the exposed materials.
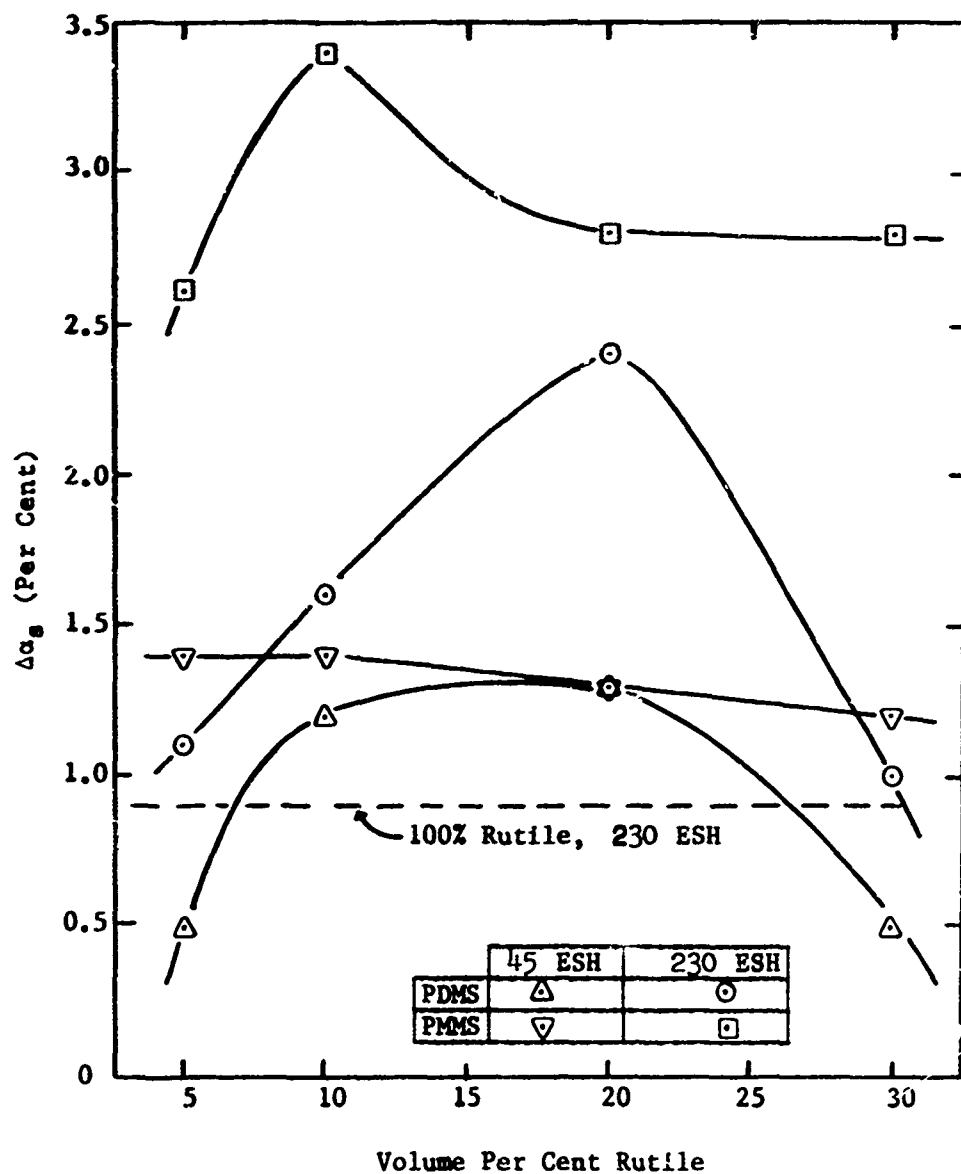
Figure 24. Effect of Pigment Concentration on Induced Solar
Absorptance in Rutile/Silicone Paints

56

Table XI. Solar Absorptance of Zinc Oxide Paint and Pigments

Sample	Material	α_s ESH = 0	$\Delta\alpha_s$ at τ ESH				
			1	2.5	11	25	120
OSP-14	ZnO	0.190	0.003	0.008	0.020	0.027	0.037
OSP -3	ZnO/PDMS	0.199	0.008	0.011	0.023	0.038	0.060
OSP -5	ZnO/PDMS	0.199	0.008	0.013	0.023	0.037	0.062
OSP -9	ZnO/PMMS	0.194	0.008	0.010	0.015	0.019	0.033
OSF-11	ZnO/PMMS	0.210	0.003	0.004	0.007	0.016	0.030

Note: The solar absorptance values shown to three places do not signify the accuracy of the reflectance measurement but merely relative degradation trends of the exposed materials.

57

Comparison of degradation rates, Fig. 25, indicate that oxygen transport through the polymethylsiloxanes had little effect on pigment stability. If oxygen transport in the binders had limited degradation, the order of increasing stability would have been ZnO < PMMS/ZnO. Solar absorptance increases for PDMS paints were greater than for PMMS paints as would be predicted by oxygen diffusion coefficients, but binderless zinc oxide stability was between that of PDMS and PMMS paints.

The smaller induced absorptances of PMMS paint compared to ZnO pigment may seem to indicate encapsulation protection. This is not substantiated by the infrared reflectance changes, Fig. 26. Reflectance changes at 2.05 μm were almost identical for ZnO pigment and PMMS paints. The greater reflectance decreases of PDMS paints in the infrared and in the visible at longer exposure times, Fig. 27, reflect instability associated with the polymer and/or pigment/polymer interaction in addition to pigment damage. All samples bleached to within 1% of the initial in-air reflectance values.

5. Zinc Orthotitanate

Surface areas and equivalent spherical particle sizes for the zinc orthotitanate powders are presented in Tables XII and XIII. Particle size of most samples increased with increasing temperature, Fig. 28. The most surprising results were the smaller particle sizes of the 1150°C-quench compared to 1050°C-quench for Samples A-5, A-6, and A-7.

Exponential size increases with increasing temperature were not expected in the loose powders. The final two-hour ball milling may have been responsible for the anomolous particle size at 1150°C. Ball milling was necessary to produce sprayable slurries of the lightly sintered powders.

Solar absorptance data, Table XIV, for the heat treated powders did not show significant UV damage trends for either quenching temperature or pigment surface area. Except for samples quenched from 1150°C and A-5, 950°C-quench, all powders had initial vacuum solar absorptances of 0.09 ± 0.01 and were fairly stable with increases in solar absorptance, $\Delta\alpha_s$, of 0.02 ± 0.005 after 230 EUVSH. Sample A-5, 950°C-quench was thin and permitted "shine through" and absorption.

The dependence of solar absorptance on temperature was apparent for pre-exposure and post-exposure reflectance studies, Fig. 29. The greatest increase in absorptance with temperature was between the 1050°C and 1150°C-quench samples. The visible region exhibited the greatest increases in absorption with temperature. Solar absorptance was identical for the 850°C-quench and anneal samples.

Ultraviolet irradiation damage to all samples was greatest in the visible region (0.45μm) and the visible damage occurred primarily in the first 20 EUVSH. Visible damage was approximately 50% recoverable while
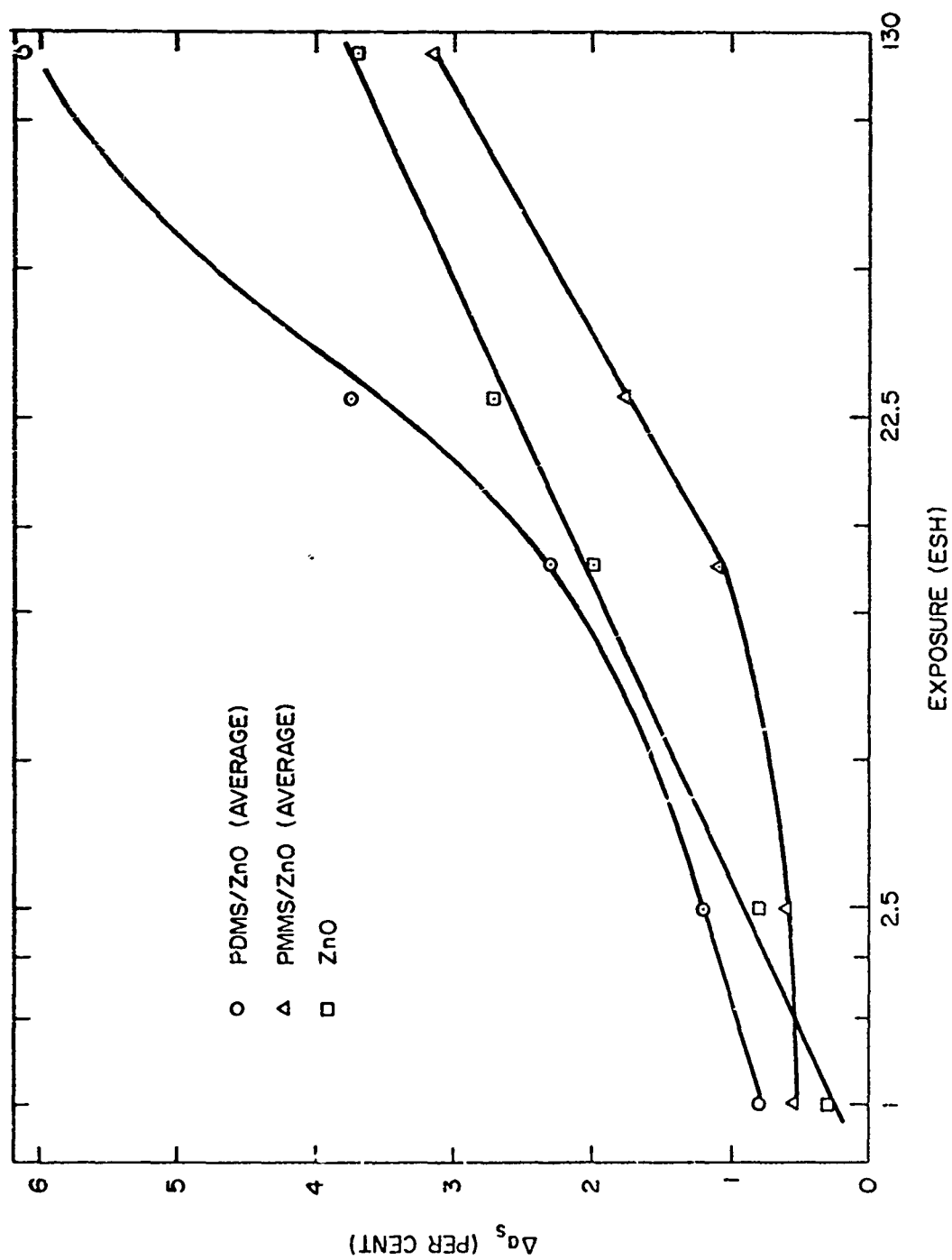
Figure 25. Ultraviolet Degradation Rates of Zinc Oxide Paints and Pigment

59
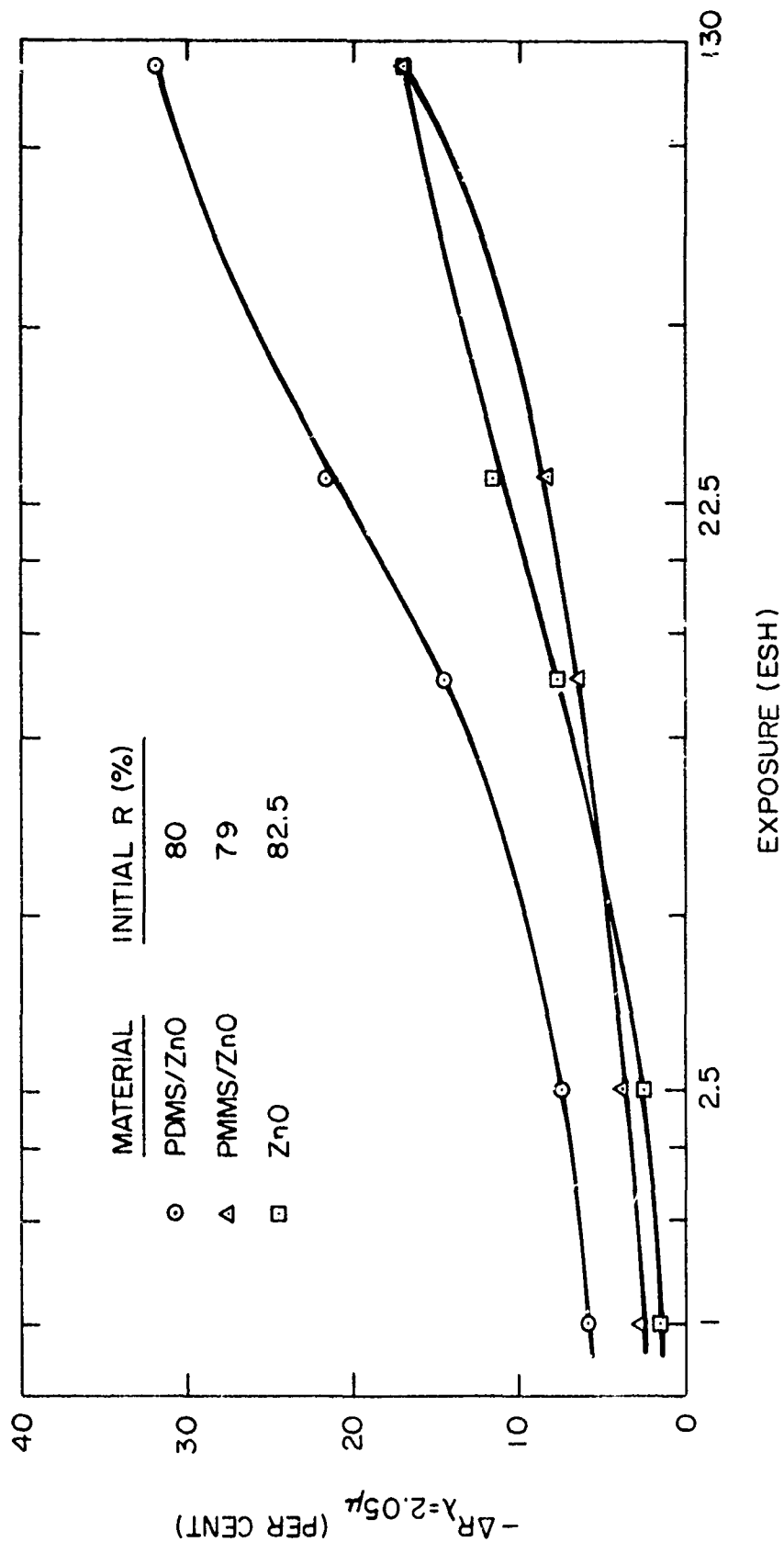
Fig. 26. Rate of Reflectance Decrease at 2.05 Microns for Ultraviolet Irradiated Zinc Oxide Paints and Pigment
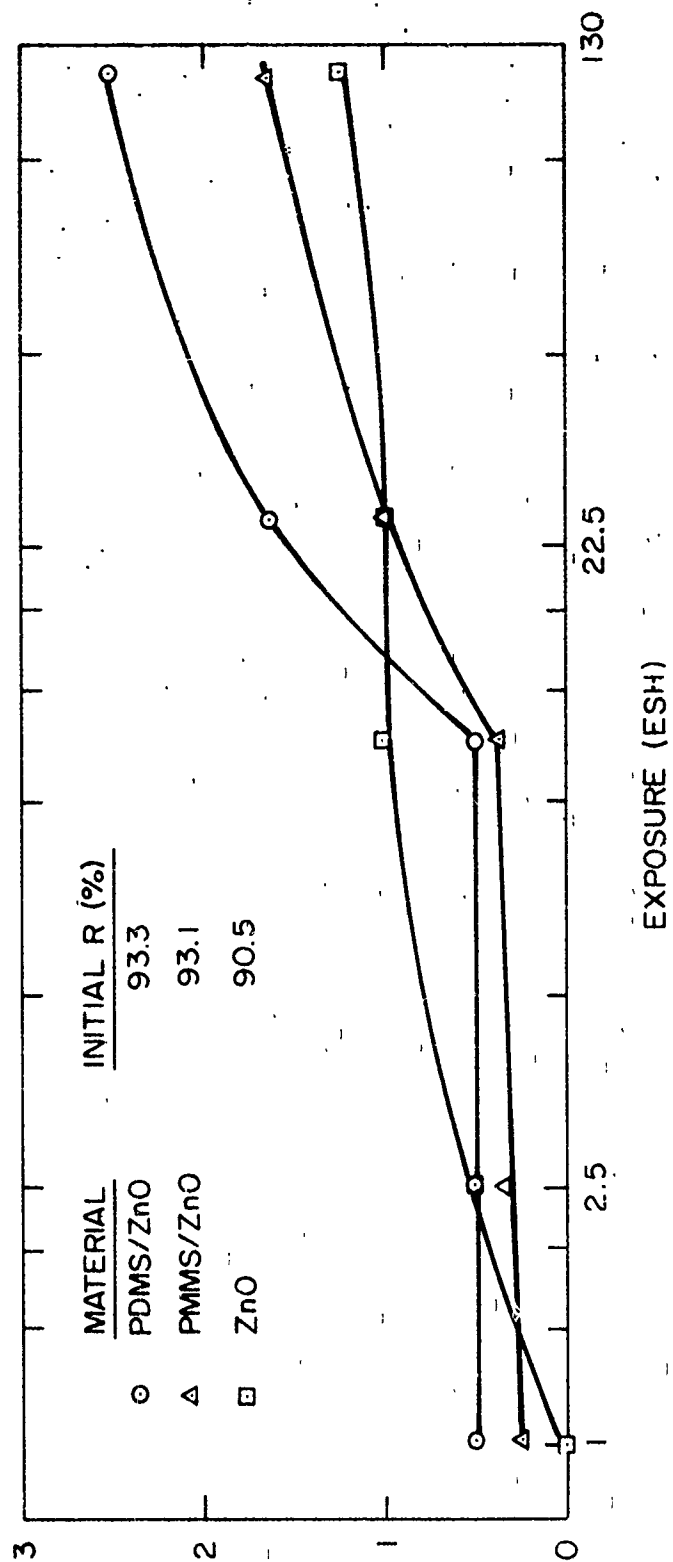
Figure 27. Rate of Reflectance Decrease at 550 nm for Ultraviolet Irradiated Zinc Oxide Paints and Pigment

Table XII. Zinc Orthotitanate Surface Areas

Heat Treatment (°C)	Surface Area (m^2/gm)			
	A-4	A-5	A-6	A-7
Before Heating	2.56	1.97	1.86	1.41
850 - Anneal	1.76	1.53	1.49	1.44
850 - Quench	2.29	1.67	1.60	1.58
950 - Quench	1.67	1.53	1.46	1.45
1050 - Quench	1.57	1.37	1.29	1.40
1150 - Quench	1.44	1.42	1.32	1.43

Table XIII. Zinc Orthotitanate Particle Sizes

Heat Treatment (°C)	Particle Size* (μm)			
	A-4	A-5	A-6	A-7
Before Heating	0.44	0.58	0.61	0.80
850 - Anneal	0.64	0.74	0.76	0.78
850 - Quench	0.50	0.68	0.71	0.72
950 - Quench	0.68	0.74	0.78	0.78
1050 - Quench	0.72	0.83	0.87	0.81
1150 - Quench	0.78	0.80	0.85	0.79

*Calculated from surface area.
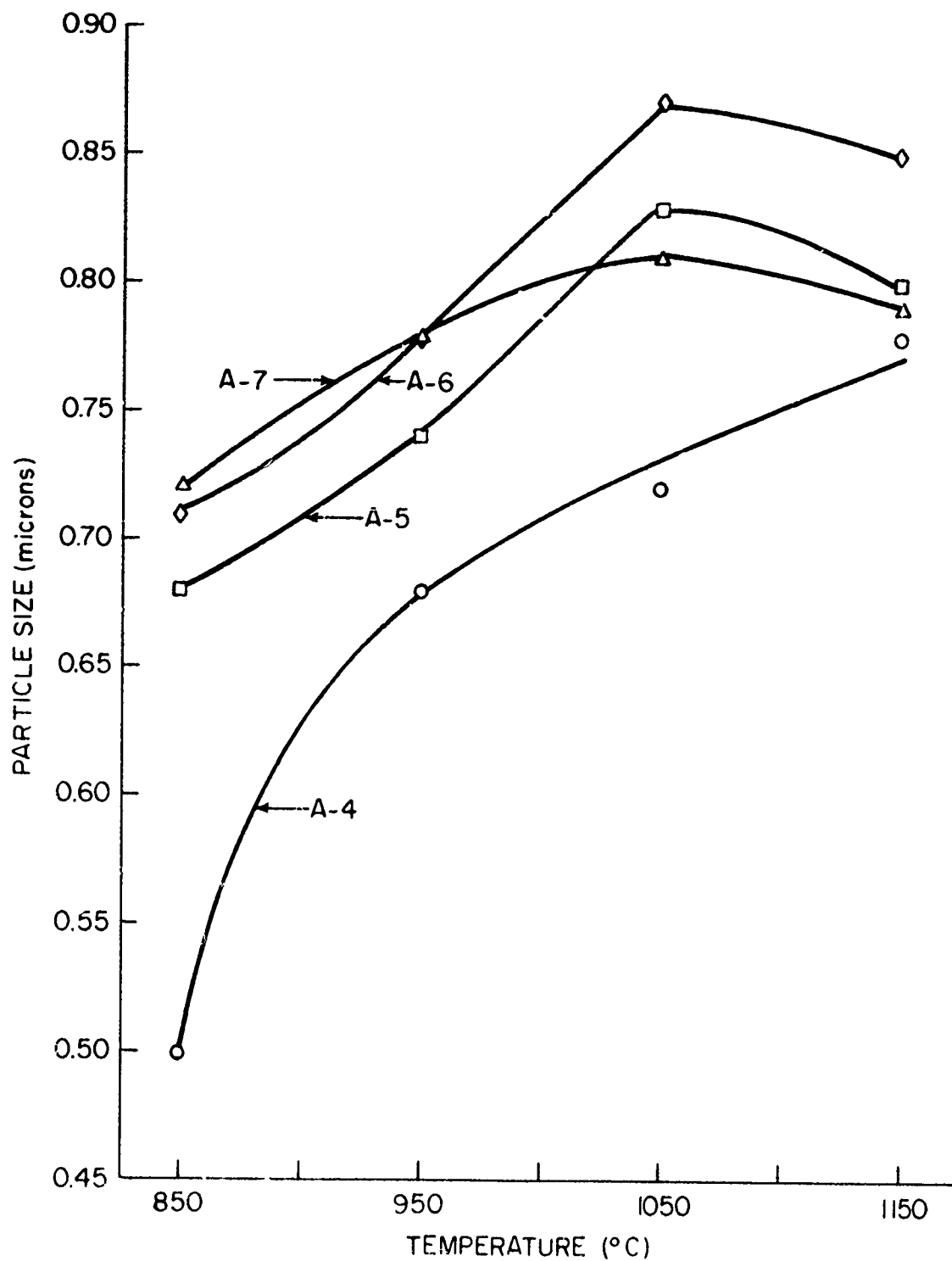
Figure 28. Effect of Temperature on Particle Size of Zn_2TiO_4 Powders

63

Table XIV. Solar Absorptance of Zinc Orthotitanate Pigments

Sample	Heat Treatment (°C)	α_s(VAC) Initial	α_s(VAC) 230 EUVSH	$\Delta\alpha_s$ (VAC)	α_s(AIR) Initial	α_s(AIR) Post Test
A-4	850-Anneal	0.086	0.106	0.020	0.084	0.089
	850-Quench	0.087	0.106	0.019	0.085	0.094
	950-Quench	0.092	0.110	0.018	0.089	0.095
	1050-Quench	0.085	0.106	0.021	0.084	0.091
	1150-Quench	0.169	0.183	0.014	0.166	0.171
A-5	850-Anneal	0.086	0.106	0.020	0.087	0.096
	850-Quench	0.086	0.107	0.021	0.084	0.093
	950-Quench *	0.120	0.135	0.015	0.108	0.124
	1050-Quench	0.103	0.124	0.021	0.105	0.111
	1150-Quench	0.147	0.160	0.013	0.148	0.150
A-6	850-Anneal	0.080	0.096	0.016	0.074	0.084
	850-Quench	0.080	0.101	0.021	0.079	0.092
	950-Quench	0.085	0.102	0.017	0.088	0.095
	1050-Quench	0.094	0.116	0.022	0.096	0.101
	1150-Quench	0.125	0.145	0.020	0.129	0.133
	850-Anneal	0.085	0.108	0.022	0.088	0.098
	850-Quench	0.083	0.102	0.019	0.080	0.092
	950-Quench	0.092	0.116	0.024	0.095	0.103
	1050-Quench	0.090	0.112	0.022	0.091	0.097
	1150-Quench	0.125	0.148	0.023	0.129	0.136

* Thin sample permitted "shine through" and absorption.

Note: The solar absorptance values shown to three places do not signify the accuracy of the reflectance measurement but merely relative degradation trends of the exposed materials.
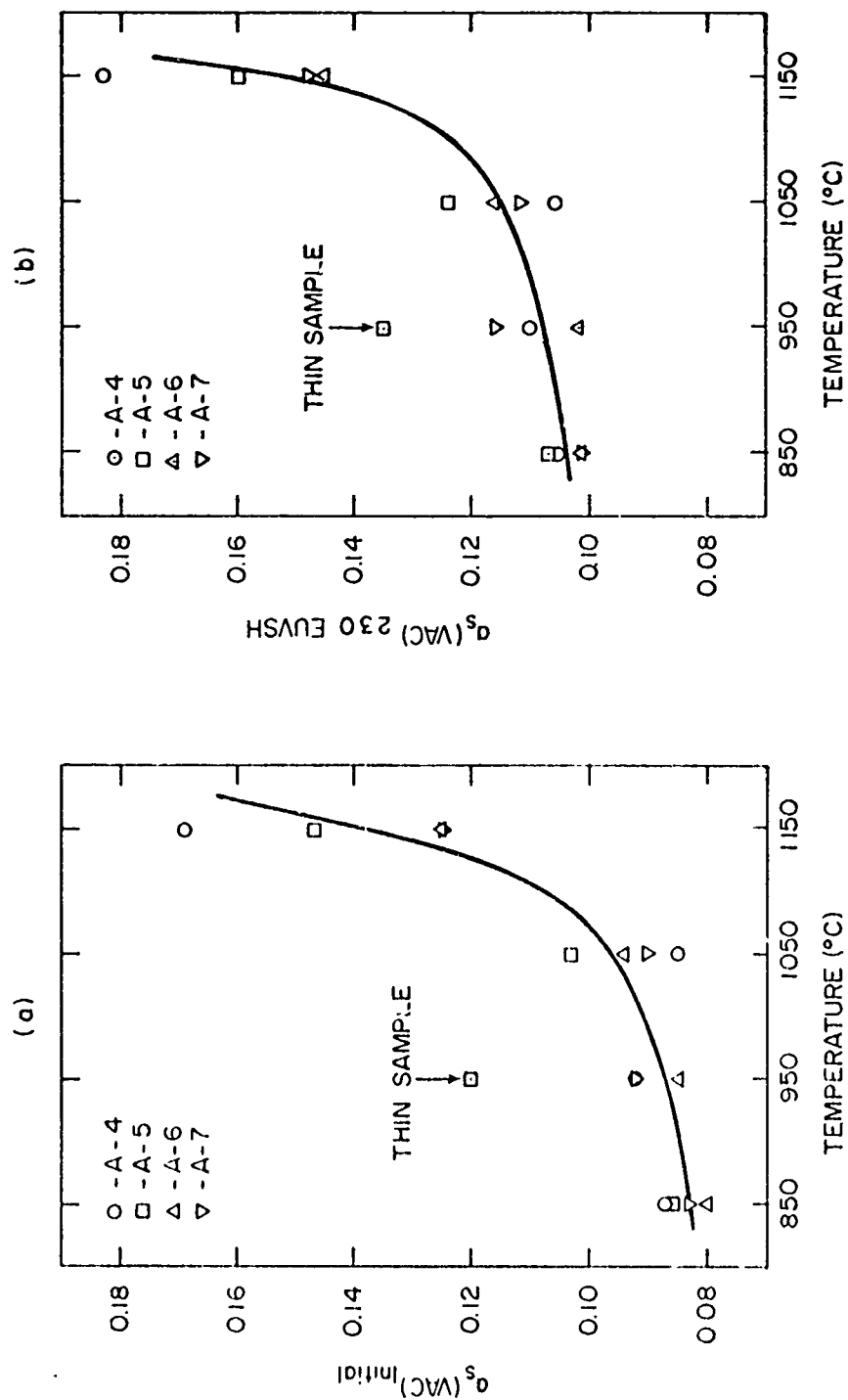
Figure 29. In Situ Solar Absorptance as a Function of Temperature for Zn_2TiO_4 (a) Prior to irradiation and (b) after 230 EUVSH

65

damage in the infrared (0.8 to 1.0 μm) recovered completely on air exposure.

Lack of damage dependence on ball milling time (A-4 to A-7 series) was surprising. Both grinding-induced strain and chemical contamination increased with milling time and would be expected to contribute to degradation cf the pigments.

V. CONCLUSIONS

Investigation of thermal control coatings composed of polymethyl-siloxanes pigmented with rutile and zinc oxide resulted in the following conclusions:

1. Oxygen adsorption on rutile was present in polydimethyl-siloxane and not in polymonomethylsiloxane.

2. For gas solution in the polymer and on the pigment, heats of solution may be predicted by assuming separate non-interacting phases.

3. Rayleigh's structure factor successfully predicted the effect of pigmentation on permeability and diffusion constants.

4. Pigment-polymer surface interaction did not measurably affect ultraviolet induced solar absorptance.

5. Oxygen transport in the polymers was too high to limit induced solar absorptance of the pigment.

Ultraviolet irradiation of zinc orthotitanate powders of varying particle size and quenched from various temperatures resulted in the following conclusions:

1. Particle size and heat treatment temperature had no observable affect on ultraviolet degradation of the pigments.

2. Pre-irradiation and post-irradiation solar absorptance increased with quenching temperature.

VI. REFERENCES

1. Wendlant, W. W., and Hecht, H. G., Reflectance Spectroscopy: Chemical Analysis, Vol. 21, Interscience Publishers, New York, pp. 62-63, (1965).

2. Johnson, F. S., "The Solar Constant," Journal of Meteorology, 11, pp. 431-439, (1954).

3. Fogdall, L. B., and Cannaday, S. S., "Ultraviolet and Electron Radiation Effects on Reflectance and Emittance Properties of Thermal Control Coatings," Technical Report AFML-TR-70-156, Air Force Contract F33615-69-C-1238, The Boeing Company, Seattle, Washington, p. 27, (July, 1970).

4. Pearson, B. D., "Preliminary Results from the Ames Emissivity Experiment on OSO-II," Progress in Astronautics and Aeronautics: Thermophysics and Temperature Control of Spacecraft and Entry Vehicles, Vol. 18, Academic Press, Inc., New York, pp. 459-472.

5. Lewis, D. W. and Thostesen, T. O., "Mariner-Mars Absorptance Experiment," Progress in Astronautics and Aeronautics: Thermophysics and Temperature Control of Spacecraft and Entry Vehicles, Vol. 18, Academic Press, Inc., New York, pp. 441-457, (1965).

6. Macmillan, H. F., Sklensky, A. F., and McKellar, L. A., "Apparatus for Spectral Bidirectional Reflectance Measurements during Ultraviolet Irradiation in Vacuum," Progress in Astronautics and Aeronautics: Thermophysics and Temperature Control of Spacecraft and Entry Vehicles, Vol. 18, Academic Press, Inc., New York, pp. 129-149, (1965).

7. Zerlaut, G. A. and Courtney, W. J., "Space-Simulation Facility for In Situ Reflectance Measurements," Progress in Astronautics and Aeronautics: Thermophysics of Spacecraft and Planetary Bodies, Vol. 20, Academic Press, New York, pp. 349-368, (1967).

8. Neel, C. B., "Role of Flight Experiments in the Study of Thermal-Control Coatings for Spacecraft," Progress in Astronautics and Aeronautics: Thermophysics of Spacecraft and Planetary Bodies, Vol. 20, Academic Press, New York, pp. 411-438, (1967).

9. Millard, J. P., "Results from the Thermal Control Coatings Experiment on OSO-III," Progress in Astronautics and Aeronautics: Thermal Design Principles of Space and Entry Bodies, Vol. 21, Academic Press, New York, pp. 769-795, (1969).

10. Arvesen, J. C., "Spectral Dependence of Ultraviolet-Induced Degradation of Coatings for Spacecraft Thermal Control," Progress in Astronautics and Aeronautics: Thermophysics of Spacecraft and Planetary Bodies, Vol. 20, Academic Press, New York, pp. 265-280, (1967).

11. Slemp, W. S. and Hankinson, T. W. E., "Environmental Studies of Thermal Control Coatings for Lunar Orbiter," Progress in Astronautics and Aeronautics: Thermal Design Principles of Space and Entry Bodies, Vol. 21, Academic Press, New York, pp. 797-817, (1969).

12. Caldwell, C. R. and Nelson, P. A., "Thermal Control Experiments on the Lunar Orbiter Spacecraft," Progress in Astronautics and Aeronautics: Thermal Design Principles of Space and Entry Bodies, Vol. 21, Academic Press, New York, pp. 819-852, (1969).

13. Gilligan, J. E., "The Optical Properties Inducible in Zinc Oxide," Progress in Astronautics and Aeronautics: Thermophysics of Spacecraft and Planetary Bodies, Vol. 20, Academic Press, New York, pp. 329-361, (1967).

14. Medived, D. B., "Photodescription in Zinc Oxide Semiconductor," The Journal of Chemical Physics, 28, pp. 870-873, (1958).

15. Barry, T. I., and Stone, F. S., "The Reactions of Oxygen at Dark and Irradiated Zinc Oxide Surfaces," Proceedings of the Royal Society: Series A, 255, pp. 124-144, (1960).

16. Glemza, R. and Kokes, R. J., "Transient Species in Oxygen Take-Up by Zinc Oxide," Journal of Physical Chemistry, 66, pp. 566-568, (1962).

17. Ibid.

18. Blakemore, J. S., "Solar-Radiation-Induced Damage to Optical Properties of ZnO-Type Pigments," Lockheed Missiles and Space Company, Contract No. NAS8-11266, pp. 6-8, (September, 1965).

19. Sklensky, A. F., MacMillan, H. F., and Greenburg, S. A., "Solar-Radiation-Induced Damage to Optical Properties of ZnO-Type Pigments," Lockheed Missiles and Space Company, Contract No. NAS8-18114, pp. 1-11-1-15, 3-21-3-24, 4-1-4-7, (February, 1968).

20. Blakemore, J. S., "A Model for Extraterrestial Solar Degradation of Zinc Oxide," IEEE Transactions on Aerospace and Electronic Systems, Vol. 2, pp. 332-336, (1966).

21. Sklensky, loc cit.

22. Morrison, S. R., and Freund, T., "Effect of Environment on Thermal Control Coatings," S.R.I. Report No. PAD-G164, J.P.L. Contract No. 95152, Interim Report No. 1, pp. 16-19, (September, 1967).

23. Greenburg, S. A., MacMillan, H. F., and Sklensky, A. F., "Damage Mechanisms in Thermal Control Coating Systems," Lockheed Missiles and Space Company Technical Report AFML-TR-67-294, pp. 92-94, (September, 1967).

24. Ibid, pp. 78, 92.

25. Compton, D. M. J., Firle, T. E., and Neu, J. T., "Mechanisms of Degradation of Polymeric Thermal Control Coatings," Technical Report AFML-TR-68-334, Part 1, pp. 48-50, (January, 1969).

26. Greenburg, op cit, pp. 66-68.

27. Greenburg, op cit, pp. 92-94.

28. Ibid.

29. Coufova, P. and Arend, H., "The Defect Structure of Oxygen Deficient Rutile," Czechoslovak Journal of Physics, 11, pp. 845-847, (1961).

30. VonHippel, A., Kalnajo, J., and Westpahl, W. B., "Protons, Dipoles, and Charge Carriers in Rutile," Journal of Physics and Chemistry of Solids, 23, pp. 779-799, (1962).

31. Yahia, J., "Dependence of the Electrical Conductivity and Thermo-electric Power of Pure and Aluminum-doped Rutile and Equilibrium Oxygen Pressure," Physical Review, 130, pp. 1711-1719, (1963).

32. Ashford, N. A., and Zerlaut, G. A., "Development of Space-Stable Thermal-Control Coatings," IIT Research Institute Report No. U6002-77, pp. 45-52, (July, 1969).

34. Zerlaut, G. A., "Development of Space-Stable Thermal-Control Coatings," IIT Research Institute Report No. U6002-94, Contract No. NAS8-5379, p. 70, (November, 1970).

35. Personal Communication from AFML/MBE (March 1970).

36. Greenburg, op cit, pp. 55, 90-91.

37. Firle, T. E. and Flanagan, T. M., "Mechanisms of Degradation of Polymeric Thermal Control Coatings: Effects of Radiation on Selected Pigments," Gulf General Atomic Incorporated, Report No. AFML-TR-68-334, Part II, pp. 91-93, (March, 1970).

38. Zerlaut, G. A., Firestone, R. F., Rayiunas, V., Serway, R., and Rubin, G. A., "Development of Space-Stable Thermal Control Coatings," IIT Research Institute Report No. U6003-31, Contract No. NAS 8-5379, p. 7, (November, 1965).

39. Zerlaut, G. A., Noble, G., and Rodgers, F. O., "Development of Space-Stable Thermal Control Coatings," IIT Research Institute Report No. U6002-55, Contract No. NAS8-5379, pp. 65-67, (September, 1967).

40. Zerlaut, G. A. and Rubin, G. A., "Development of Space-Stable Thermal Control Coatings," IIT Research Institute Report No. U6002-36, Contract No. NAS8-5379, pp. 42-43, (February, 1966).

41. Millard, op cit, pp. 771-778.

42. Zerlaut, G. A., Noble, G., and Rogers, F. D., "Development of Space-Stable Thermal Control Coatings," IIT Research Institute Report No. U6002-59, Contract No. NAS8-4379, pp. 51-52, (January, 1968).

43. Sklensky, op cit, pp. 5-3-5-4.

44. McGinnis, W. J., U. S. Patent 3,410,708, (Novermber 12, 1968).

45. McGinnis, W. J., U. S. Patent 3,510,335, (May 5, 1970).

46. McGinnis, W. J., E. I. duPont de Nemours and Company, Pigments Division, Wilmington, Delaware, Personal Communication, (March 18, 1971).

47. Zerlaut, Fireston, Rayuinas, Serway, and Rubin, op cit, p. 6.

48. Crank, J. and Park, G. S., Diffusion in Polymers, Academic Press, New York, pp. 4-5, (1968).

49. Ibid.

50. Barrer, R. M. and Chio, H. T., "Solution and Diffusion of Gases and Vapors in Silicone Rubber Membranes," Journal of Polymer Science, 10, pp. 111-138, (1965).

51. Barrer, R. M., "Permeation, Diffusion, and Solution of Gases in Organic Polymers," Transactions of the Faraday Society, 35, pp. 628-643, (1939).

52. Stannett, V., "Simple Gases," Diffusion in Polymers, edited by Crank, J. and Park, G. S., Academic Press, New York, pp. 41-73, (1968).

53. Ibid.

54. Barrer, R. M., "Some Properties of Diffusion Coefficients in Polymers," Journal of Chemical Physics, 61, pp. 178-189, (1957).

55. Barrer, R. M. and Skirrow, G., "Transport and Equilibrium Phenomena in Gas-Elastomer Systems. I. Kinetic Phenomena," Journal of Polymer Science, 3, pp. 549-563, (1948).

56. Stannett, loc cit.

57. Scott, D. W., "Osmotic Pressure Measurements with Polydimethylsiloxane Fractions," Journal of the American Chemical Society, 68, pp. 1877-1879, (1946).

58. Ohlberg, S. M., Alexander, L. E., and Warrick, E. L., "Crystallinity and Orientation in Silicone Rubber," Journal of Polymer Science, 27, pp. 1-17, (1958).

59. Roth, W. L. and Harker, D., "The Crystal Structure of Octamethylspiro(5,5)Pentasiloxane: Rotation about the Ionic Silicon-Oxygen Bond," Acta Crystallographica, 1, pp. 34-42, (1948).

60. Kammermeyer, Karl, "Silicone Rubber as a Selective Barrier," Industrial and Engineering Chemistry, 49, pp. 1685-1686, (1957).

61. Barrer, R. M., Barrie, J. A., and Raman, N. K., "Solution and Diffusion in Silicone Rubber, II-The Influence of Fillers," Polymer, 3, pp. 605-614, (1962).

62. Barrer, R. M., Barrie, J. A., and Raman, N. K., "Solution and Diffusion in Silicone Rubber, I-A Comparison with Natural Rubber," Polymer, 3, pp. 595-703, (1962).

63. Barrer and Chio, loc cit.

64. Barrer, R. M., Barrie, J. A., and Rodgers, M. G., "Heterogeneous Membranes: Diffusion in Filled Rubber," Journal of Polymer Science, 1, pp. 2565-2586, (1963).

65. VanAmerongen, G. J., "The Effect of Fillers on the Permeability of Rubbers to Gases," Rubber Chemistry and Technology, 28, pp. 823-826, (1955).

66. Barrer, Barrie, and Rodgers, loc cit.

67. Barrer, Barrie, and Raman, "Solution and Diffusion in Silicone Rubber, II, loc cit.

68. Barrer, Barrie, and Rodgers, loc cit.

69. Rayleigh, Lord, Philosophical Magazine, 34, pp. 481-502, (1892).

70. Barrer, Barrie, and Rodgers, loc cit.

71. Barrer, Barrie, and Raman, loc cit.

72. Barrer, Barrie, and Rodgers, loc cit.

73. Zisman, W. A., "Relation of Equilibrium Contact Angle to Liquid and Solid Constitution," Contact Angle, Wettability, and Adhesion, American Chemical Society, Washington, D.C., pp. 2, 48, (1963).

74. Zisman, op cit, pp. 4-5.

75. Zisman, op cit, pp. 3-4, 36-41.

76. Adamson, A. W., Physical Chemistry of Surfaces, Second Editon, Interscience Publshers, New York, pp. 357-363, (1967).

77. Bartell, F. E., Culbertson, J. L., and Miller, M. A., "Alteration of the Free Surface Energy of Solids I," Journal of Physical Chemistry, 40, pp. 881-889, (1936).

78. Adamson, op cit, pp. 370.

79. Shafrin, E. G., and Zisman, W. A., "Upper Limits to the Contact Angles of Liquids to Solids," Contact Angle, Wettability and Adhesion, American Chemical Society, Washington, D.C., pp. 145-157, (1963).

80. Holland, L., The Properties of Glass Surfaces, Wiley, New York, pp. 434-430, (1964).

81. Moser, F., "Approximating the Attractive Forces of Adhesion for Glass and Other Surfaces," ASTM Bulletin, TP243, pp. 62-66, (1950).

82. Moser, F., "Wetting Phenomena-A Means for Determining Adhesion," The Glass Industry, pp. 201-203, 228, 232, (April, 1956).

83. Moser, F., "Polymeric Adhesives for Glass," Plastics Technology, pp. 799-805, (1956).

84. McGinnis, W. J., E. I, duPont deNemours and Company. Pigments Division, Personal Communication, (March 29, 19.).

85. Burzynski, A. J., and Martin, F. E., U.S. Patent 3,394,114. (June 18, 1968).

86. Campbell, W. F., and Cochran, R. L., "Degradation Mechanisms of Pigmented Coatings," Technical Report APML-TR-71-2, Pt. 1, pp. 3-7 (March, 1970).

87. Gagnon, D. W., Chemical & Polymer Development, Owens-Illinois, Toledo, Ohio, Personal Communication, (August, 1970).

88. Campbell, op cit, pp. 28-37.

89. Bartell, F. E., and Zuidema, H. H., "Wetting Characteristics of Low Surface Tension Such as Talc, Waxes, and Resins," Journal of American Chemical Society, 58, pp. 1449-1454, (1942).

90. Dettre, R. H., and Johnson, R. E., "Contact Angle Hysteresis, II. Contact Angle Measurements on Rough Surfaces," Contact Angle, Wettability, and Adhesion, American Chemical Society, Washington, D. C., pp. 136-144, (1964).

91. Adamson, A. W., Physical Chemistry of Surfaces, Second Edition, Interscience Publishers, New York, pp. 357-363, (1967).

92. Bartell, F. E., Culbertson, J. L., and Miller, M. A., "Alteration of the Free Surface Energy of Solids I," Journal of Physical Chemistry, 40, pp. 881-889, (1936).

93. Shafrin, E. G., and Zisman, W. A., "Upper Limits to the Contact Angles of Liquids to Solids," Contact Angle, Wettability, and Adhesion, American Chemical Society, Washington, D.C., pp. 145-157, (1963).

94. Moser, F., "Approximating the Attractive Forces of Adhesion for Glass and Other Surfaces," ASTM Bulletin, TP248, pp. 62-66, (1950).

95. Zerlaut, G. A., and Rubin, G. A., "Development of Space-Stable Thermal Control Coatings," IIT Research Institute Report No. U6002-NAS8-5379, pp. 42-43, (February, 1966).

96. Zerlaut, G. A., "Development of Space-Stable Thermal Control Coatings," IIT Research Institute Report No. U6002-94, NAS8-5379, pp. 70-71, (November, 1970).

97. Campbell, AFML-TR-71-42, Pt. 1, op cit, pp. 26-32.

APPENDIX

OXYGEN TRANSPORT DATA

Preceding page blank

Table XV - Effect of Pressure on Oxygen Transport Constants in
Polydimethylsiloxane at 25°C

Polydimethylsiloxane

P (cm Hg)	P (cc(STP)/sec/cm²/cm/cm Hg)	D (cm²/sec)	S (cc(STP)/cc/atm)	V (cc(STP)/cc)
19.6	7.69×10^{-9}	18.9×10^{-6}	0.309	0.079
30.6	7.67	18.8	0.310	0.125
39.6	7.66	18.5	0.314	0.165
49.7	7.80	19.0	0.311	0.203
59.9	7.90	19.3	0.311	0.245

Table XVI - Effect of Pressure on Oxygen Transport Constants in
Polymonomethylsiloxane at 25°C

P (cm Hg)	p (cc(STP)/sec/ cm²/cm Hg)	D (cm²/sec)	S (cc(STP)/ cc/atm)	V (cc(STP)/cc)
Polymonomethylsiloxane				
19.5	2.71×10^{-9}	4.98×10^{-7}	0.413	0.106
30.5	2 86	5.07	0.428	0.172
39.6	1.85	4.87	0.445	0.231
49.5	2.87	5.05	0.432	0.281
59.6	2.85	5.14	0.421	0.331

Table XVII - Oxygen Transport Constants for Oxygen in
Polymonomethylsiloxane/Rutile Compositions

T ($°C$)	$P \times 10^9$ (cc(STP)sec/ cm^2/cm/cm Hg)	$D \times 10^7$ (cm^2/sec)	S (cc(STP)/ cc/atm)
Sample 10-0% Rutile			
0	1.68	2.68	0.476
25	2.83	5.02	0.428
32	3.29	5.55	0.450
50	4.72	7.92	0.453
60	5.95	10.2	0.443
Sample 11-5.2% Rutile			
0	1.34	2.49	0.409
25	2.26	4.56	0.376
32	2.70	5.02	0.409
50	3.86	7.52	0.390
60	4.35	8.25	0.401
Sample 12-10.4% Rutile			
25	2.13	4.06	0.399
32	2.44	4.51	0.411
50	3.54	6.66	0.404
60	4.22	7.62	0.421
Sample 13-20.7% Rutile			
0	0.95	2.09	0.348
25	1.87	3.78	0.378
32	2.08	4.65	0.341
50	3.05	6.36	0.364
60	3.86	8.13	0.366